Detecting patterns of upwelling variability in Eastern Boundary Upwelling Systems with special emphasis on the Benguela region

Amieroh Abrahams

UNIVERSITY *of the* WESTERN CAPE

DEPARTMENT OF BIODIVERSITY & CONSERVATION BIOLOGY

A thesis submitted in fulfilment of the requirements for the degree of Magister Scientiae in the Department of Biodiversity and Conservation Biology, Faculty of Science, University of the Western Cape

Supervisor: Prof. A.J. Smit
Co supervisor: Dr. Robert Schlegel
15 September 2020

KEYWORDS

Code:R

In situ data

Ocean

Remotely-sensed data

Upwelling

Wind

ABSTRACT

Detecting patterns of upwelling variability in EBUS with special emphasis on the Benguela region

A. Abrahams

MSc. Thesis, Department of Biodiversity and Conservation Biology, University of the Western Cape.

Coastal upwelling is one of the most important oceanographic processes relating to ecosystem function at local and global spatial scales. To better understand how changes in upwelling trends may occur in the face of ongoing anthropogenically induced climate change it is important to quantify historical trends in climatic factors responsible for enabling coastal upwelling. However, a paucity of conclusive knowledge relating to patterns concerning changes in upwelling across the world's oceans over time makes such analyses difficult. In this study I aimed to quantify these patterns by first identifying when upwelling events occur using a novel method for predicting the behaviours of coastal upwelling systems over time. By using remotely sensed SST data of differing resolutions as well as several wind variables I was able to identify and quantify upwelling signals at several distances away from the coastline of various upwelling systems. Using this novel method of determining upwelling, I then compared upwelling patterns within all Eastern Boundary Upwelling Systems (EBUS) over a period of 37 years, with the assumption that climate change was likely to have driven variable wind patterns leading to a more intense upwelling over time. Overall, upwelling patterns and wind variables did not intensify overtime. This method of identifying upwelling may allow for the development of predictive capabilities to investigate upwelling trends in the future.

DECLARATION

I declare that "**Detecting patterns of upwelling variability in EBUS with special emphasis on the Benguela region**" is my own work, that it has not been submitted for any degree or examination at any university, and that all sources I have used or quoted have been indicated and acknowledged by complete references.

Full name: Amieroh Abrahams **Date:** 15 September 2020

Signature: 

ACKNOWLEDGEMENTS

I would like to acknowledge my supervisors. The support provided by them during this process were only surpassed by their insight into the methods allowing the production of this research. Additionally, I would also like to acknowledge all of the sources that contributed to the collection of the *in situ* coastal temperature data used in the second chapter of this thesis. This research was supported by the National Research Foundation Grant (SFH180604339745).

PREFACE

This Master's thesis covers the research I have performed over the last two years. This printed body of work is static in nature, the data science upon which it has been built is not. Much of this work may be found at my GitHub page: https://github.com/AmierohAbrahams/Upwelling_MCS.

TABLE OF CONTENT

ABSTRACT 5
DECLARATION 6
ACKNOWLEDGEMENTS 7
PREFACE 9
TABLE OF CONTENT 10
LIST OF FIGURES 11
LIST OF TABLES 13
CHAPTER 1 15
GENERAL INTRODUCTION 15
1.1. EBUSs and the Benguela upwelling system 16
1.2. Upwelling 16
1.2.1. Atmospheric drivers of upwelling 16
1.2.2. Upwelling dynamics 16
1.2.3. Trends 17
1.2.4. Climate Change 18
1.2.5. The Bakun Hypothesis 19
1.3. Extreme events in the context of upwelling 19
1.4. Rationale 19
1.4.1. Predictions/Hypotheses 19
CHAPTER 2 21
UPWELLING SIGNALS: A COMPARISON OF SEA SURFACE TEMPERATURE IN THE BENGUELA 21
Abstract 22
2.1. Introduction 23
2.2. Methods 24
2.2.1. Site Selection 24
2.2.2 Datasets 25
2.2.3 Wind data 25
2.2.4 Defining and determining upwelling 25
2.3. Results 26
2.4. Discussion 35
2.4.1 Data products 35
2.4.2. Oceanography 36
2.4.3 Conclusion 37
CHAPTER 3 38
VARIATION OF UPWELLING SIGNALS DETECTED IN EBUS 38
Abstract 39
3.1. Introduction 40
3.2. Methods 41
3.2.1. Data 41
3.2.2. Upwelling identification 41
3.3. Results 42
3.4. Discussion 47
CHAPTER 4 50
SYNTHESIS AND CONCLUSION 50
4.1. Contributions 51
4.2. Further research 52
REFERENCES 53

Figure 2.1: Map of southern Africa showing and coastal bathymetry. The black points represent the location of the *in situ* temperature sites and the empty red boxes show the pixels used along the shore normal transect from the satellite sea surface temperatures (SST) time series. The red boxes are at 0 km, 25 km and 50 km from the coastline. 24

Figure 2.2: The upwelling duration for each of the signals detected for the four satellite products and the SACTN *in situ* collected data during summer months (December, January and February), over a four-year period. 27

Figure 2.3: The mean intensity for each of the signals detected for the four satellite products and the SACTN *in situ* collected data during summer months (December, January and February), over a four-year period..... 28

Figure 2.4: The upwelling cumulative intensity for each of the signals detected for the four satellite products and the SACTN *in situ* collected data during summer months (December, January and February), over a four-year period. 29

Figure 2.5: The duration for each of the signals detected at the various distances from the shore for the four satellite products during summer months (December, January and February), over a four-year period. 30

Figure 2.6: The mean intensity for each of the signals detected at the various distances from the shore for the four satellite products during summer months (December, January and February), over a four-year period..... 30

Figure 2.7: The cumulative intensity for each of the signals detected for the four satellite products during summer months (December, January and February), over a four-year period..... 31

Figure 2.8: The duration of upwelling signals detected for the four satellite products at the different distances from the shore during summer months (December, January and February), over a four-year period. 32

Figure 2.9: The mean intensity for each of the signals detected for the four satellite products at difference distances from the shore during summer months (December, January and February), over a four-year period. 33

Figure 2.10: The cumulative intensity for each of the signals detected for the four satellite products at difference distances from the shore during summer months (December, January and February), over a four-year period. 34

Figure 2.11: The average number of the signals detected at each site for the various satellite products from 2011 until 2014. 35

Figure 3.1: OISST throughout the global ocean. The red coloured squares delimit EBUS: A: California (CCS), B: Humboldt (HCS), C: Canary (CnCS) and D: Benguela (BCS) current systems. 41

Figure 3.2: SST trends during austral (DJF) and boreal (JJA) summer months over 37 year. 43

Figure 3.3: Counts of south-easterly directed winds during austral (DJF) and boreal (JJA) summer months over a period of 37 year. 44

Figure 3.4: Duration of south-easterly directed winds during austral (DJF) and boreal (JJA) summer months over a period of 37 year. 44

Figure 3 5: The intensity of south-easterly directed winds during austral (DJF) and boreal (JJA) summer months over a period of 37 year. 45

Figure 3.6: Number of upwelling signals detected during austral (DJF) and boreal (JJA) summer months over a period of 37 year. 45

Figure 3.7: Mean intensity of upwelling signals detected during austral (DJF) and boreal (JJA) summer months over a period of 37 year. 46

Figure 3.8: Cumulative intensity of upwelling signals detected during austral (DJF) and boreal (JJA) summer months over a period of 37 year. 46

LIST OF TABLES

Table 2.1: Metrics of upwelling signals and their descriptions. 26

Table 2.2: One-way ANOVA evaluating the variation in the duration of upwelling signals detected in the various gridded SST and *in situ* products between four sites within the Benguela Current region of South Africa. Comparisons are graphically captured in **Figure 2.2**..... 27

Table 2.3: One-way ANOVA evaluating the variation in the mean intensity of upwelling signals detected in the four gridded SST and *in situ* products between the four sites within the Benguela Current region of South Africa. Comparisons are graphically captured in **Figure 2.3**..... 27

Table 2.4: One-way ANOVA evaluating the variation in upwelling cumulative intensity as detected in the four gridded SST and *in situ* products between four sites within the Benguela Current region of South Africa. Comparisons are graphically captured in **Figure 2.4**. 28

Table 2.5: One-way ANOVA evaluating the variation in the duration of upwelling signals detected at the various distances from the shore for the four gridded SST product between at the various distances from the shore. Comparisons are graphically captured in **Figure 2.5**..... 29

Table 2.6: One-way ANOVA evaluating the variation in the mean intensity of upwelling signals detected in the four gridded SST product between at the various distances from the shore. Comparisons are graphically captured in **Figure 2.6**. 30

Table 2.7: One-way ANOVA evaluating the variation in the cumulative intensity of upwelling signals at the various distances from the shore detected in the four gridded SST product between at the various distances from the shore. Comparisons are graphically captured in **Figure 2.7.**..... 31

Table 2.8: Nested ANOVA evaluating the variation in upwelling duration as detected in four gridded SST products (OISST, CMC, G1SST, and MUR) at several distances away from the shore and sites within the Benguela Current region of South Africa. Only the main effect due to 'product' is indicated. Comparisons are graphically captured in **Figure 2.8**. 32

Table 2.9: Nested ANOVA evaluating the variation in the mean intensity of upwelling signals are detected in four gridded SST products (OISST, CMC, G1SST, and MUR) at several distances away from the shore and sites within the Benguela Current region of South Africa. Only the main effect due to 'product' is indicated. Comparisons are graphically captured in **Figure 2.9**. 32

Table 2.10: Nested ANOVA evaluating the variation in upwelling cumulative intensity as detected in four gridded SST products (OISST, CMC, G1SST, and MUR) at several distances away from the shore and sites within the Benguela Current region of South Africa. Only the main effect due to 'product' is indicated. Comparisons are graphically captured in **Figure 2.10**. 33

Table 2.11: A Pearson correlation of the relationship between the number of signals detected at a distance of 0 km versus a distance of 25 km and between the number of signals at 0 km and 50 km. 34

Table 3.1: Linear regressions displaying yearly differences in south-easterly (SE) directed winds and upwelling metrics over a period of 37 years. 43

CHAPTER 1

GENERAL INTRODUCTION

1.1. EBUSs and the Benguela upwelling system

Globally, there are four major Eastern Boundary Upwelling Systems (EBUS) distributed throughout western coastlines across the world's oceans. This includes the Benguela Current off south-western Africa; the Canary Current off north-western Africa, together with its northern extension off the Iberian Peninsula of south-western Europe; the Peru-Humboldt Current off western South America; and the California Current off the western continental USA and north-western Mexico (Bakun,1990; Pauly and Christensen, 1995; Bakun et al., 2015). Each of these systems are characterised as vast regions of coastal ocean that contain upwelled water located on the eastern side of their respective ocean basins. While these regions cover only 1% of the world's ocean surface, they are among the most productive regions of the ocean (Pauly and Christensen, 1995). This is due to these systems being subject to intensive coastal upwelling that brings cold, nutrient rich, high concentrated CO2, low pH, and low oxygenated waters to the surface (Pauly and Christensen, 1995). As consequences of this upwelling, diverse marine fauna and flora are able to thrive in these areas due to the abundance of available nutrients.

The Benguela Upwelling System (BUS) is one of the most productive upwelling areas in the world ocean. The cold Benguela Current waters are bound in the south by the warm Agulhas retroflexion region and in the north by the southward flowing Angola current. The Benguela system is split into northern and southern systems by a zone of intense perennial upwelling activity in Lüderitz within the Namibian region (Shannon, 1986; Cole, 1999). The flow of the Benguela Current is considered to be topographically guided (Nelson and Hutchings, 1983; Barange, 1991). The region surrounding the Benguela Current experiences a persistent alongshore wind which is associated with the St. Helena high pressure system (Guastella, 1992; Schultz, 2010). The continental shelf bathymetry and upwelling favourable winds provide a large-scale upwelling mechanism in the Benguela Current, whereas local bathygraphy and meteorology creates an alternating pattern of active and passive upwelling circulations along the coast (Chaigneau et al., 2009; Gutknecht et al., 2013). Upwelling occurring along the south coast of the Western Cape Province of South Africa, is generated by local winds which increase away from the coast (Fennel et al., 1999).

1.2. Upwelling

1.2.1. Atmospheric drivers of upwelling

EBUS forms part of the wind-driven ocean circulation. Their existence and dynamics are driven by wind direction and strength that cause Ekman transport that cannot be balanced by the horizontal advection of water (Bakun and Weeks, 2004; Capet et al., 2004). For nearly a century we have known that Ekman transport forced by equatorward upwelling-favourable winds is the main driver of the greatest eastern coastal upwelling systems (Sverdrup and Allen, 1939). During summer, when sea surface temperatures (SST) are warm, upwelling can be observed as a local temperature drop (Gurova et al., 2013), with a typical time series of upwelling ranging from a few days to a few weeks. The wind responsible for coastal upwelling is dependent on pre-existing pressure gradients that respond to large-scale changes in global circulation like the location and intensity of subtropical anticyclones and associated trade winds, as well as to local processes associated with the establishment of thermal low pressure systems over the continents in the warm seasons (García-Reyes et al., 2015; Walker, 2020). Typically, upwelling favourable winds are caused by cross-shore atmospheric pressure gradients, and these gradients occur predominantly during heating periods.

Regions surrounding the Benguela EBUS, are dominated by anticyclonic high-pressure cells with quasi-stationary positions, resulting in abundant southerly and south easterly winds (Risien et al., 2004; Hagen et al., 2009). The South Atlantic Ocean High is situated along the west coast, drawing cool, dry air onto the west of the subcontinent (Van Heerden and Hurry, 1998). Solar heating during summer may result in the development of low-pressure cells known as heat lows which are absent during the winter (Tyson and Preston-Whyte, 2000). As the anticyclones shift north during winter months, the cold westerlies substantially impact on the weather of the southern tip of the South African subcontinent (Van Heerden and Hurry, 1998). Further offshore, the wind stress curl causes upwelling by Ekman pumping. The coastal topography and the climatological winds frame the areas of upwelling (Shannon, 1985; Chavez and Messié, 2009).

1.2.2. Upwelling dynamics

El Nino-Southern Oscillation (ENSO) is characterised by interannual SST variations. However, ENSO SST anomalies could also be derived from the central equatorial Pacific and spread toward the eastern Pacific (e.g., Wang 1995). This led to the suggestion that there may be more than one type of ENSO in the tropical Pacific, and the changes of the propagation direction may be a result of the alternation of different types of ENSO dynamics, such as the slow-SST type

(Neelin 1991; Jin and Neelin 1993a,b) and the delayed-oscillator type (Schopf and Suarez 1988; Suarez and Schopf 1988; Battisti and Hirst 1989). ENSO events were usually classified according to their periodicity, propagation direction, onset time, or the associated zonal SST structure (e.g., Yasunari 1985; Fu et al. 1986; Barnett et al. 1991; Enfield and Cid 1991; Xu and Chan 2001). However, it appears that the shift of the SST anomaly centre between the eastern and central equatorial Pacific is a common contrasting feature among these various types of ENSO. During ENSO, the Trade winds are weakened or reversed, and as a result, central Pacific upwelling is turned into downwelling, creating a warm layer of SST (Klein et al., 1999; Wang and McPhaden, 2000; Beaufort et al., 2001).

EBUS have common properties (Blanco, 2001), where under typical conditions the main transport carries cold, well-oxygenated water from high towards low latitudes. The well-known Pacific El Niño (EN) is manifest as an episodic warming of coastal waters off Peru. The ENSO caused marked changes in precipitation and wind patterns in the South-East Atlantic (Bakun, 1996; Shannon et al., 1996). The Humboldt Current (Peru-Chile) and California Current, systems are both directly impacted from EN and La Niña (LN) (i.e. the warm and cold phases of the ENSO cycle) (Halpern, 2002; Arntz et al., 2006; Vargas et al., 2007). The Canary Current however is unique in that it does not have an oxygen minimum zone (OMZ) (Arístegui et al., 2009; Pelegrí and Peña-Izquierdo, 2015). OMZ is mainly affected by warm and cold phases of the ENSO. During EN, intra-seasonal Equatorial Kelvin Waves (IEKW) are generated by wind anomalies in the Equatorial Pacific region (Kessler et al., 1995). They propagate eastward and reach the western coasts of the Americas (Gushchina et al., 2012). There, they trigger coastal trapped waves (CTWs) which propagate poleward and impact the vertical structure of physical and biogeochemical variables alongshore off Peru (Echevin et al., 2014; Graco et al., 2017) and Chile (Ulloa et al., 2001). The water column thus becomes oxygenated during EN and a deeper oxycline (>100 m) is observed, while during LN (e.g., 1999–2000), a shallower oxycline is described (Morales et al., 1999).

Coastal upwelling within the Humboldt current exhibits strong interannual variability forced by the ENSO cycle, especially to its warm phase EN (Escribano et al., 2004). Oceanographic changes included the intrusion of oceanic, low-nutrient, and highly oxygenated waters into the coastal areas, with positive SST anomalies. Three main features are present under EN conditions, (i) raise in sea surface temperature, (ii) change of water mass distribution toward the coast, and (iii) decrease of primary production. Although upwelling-favourable winds can increase during EN and the depth of the upwelling source waters can remain rather unaffected, the nutrient supply to surface waters often decreases as the result of complex physical processes that involve downwelling and offshore transport, consequently primary production is reduced under such scenarios (Espinoza-Morriberon et al., 2017). The main physical processes connecting ENSO with the northern upwelling region are related to thermocline perturbations and changes in the alongshore currents forced by equatorial kelvin waves (Shaffer et al., 1997).

The Benguela region expresses the Benguela Niños and are less frequent and intense than the Pacific events (Cury and Shannon, 2004; Florenchie et al., 2004). Benguela Niños are defined as anomalous warm events occurring between the southward flowing Angola current and the BUS off south western Africa (Shannon, 1986). The annual southward migration of the Angola Benguela front introduces warm, saline Angolan water into Namibian coastal water. This seasonal migration is associated with the relaxation of the equatorward, upwelling-favourable wind stress (Boyd et al., 1987), while the southward penetration of warm saline water during the Benguela Niño does not seem to be associated with local winds (Stander and De Decker, 1969). Evidently, Benguela Niños are expressed as regions of abnormal, persistent high SST. Many researchers often associate the equatorial interannual variability pattern in the Atlantic to the ENSO phenomenon (Zebiak, 1993; Sutton et al., 2000). Servain (1985) suggested that eastern tropic oceans are governed by remote wind stress effects through equatorial wave dynamics. The Benguela Niño is believed to be associated with large-scale remote changes in the wind patterns. Hence, anomalies in trade winds may result in Kelvin waves that propagate eastward along the equator, inducing a deepening or a lifting of the thermocline. These warm events are also known to impact fisheries and the climate of this region and are also proven to induce unexpected rainfall events and drastically influence fish abundance and distribution (Boyer and Hampton, 2001; Rouault et al., 2003).

In general, regional ocean climate oscillations like the ENSO and Benguela Niño for the Benguela Current System show considerable variability in temperatures (Minobe et al., 1999) and complicated attempts to assess long term trends (Rimbu et al., 2003). However, many of the trends in recent decades might be associated with these oscillations (Barton et al., 2013). Some of these climate oscillations are expected to increase in amplitude or variance with climate change (Timmerman et al., 1999; Sydeman et al., 2013) which would further influence future trend

1.2.3. Trends

Research examining the trends in upwelling favourable winds have found variable results. This is due to small amplitude of uni-directional wind trends relative to amplitudes of seasonal and decadal wind variability, the short

duration of time series relative to decadal variability, inconsistencies in data treatment and changes in measurement techniques used to interpolate or reanalyse data (Cardone et al., 1990). Sydeman et al. (2014) find a more accurate pattern of intensifying upwelling favourable winds in the Humboldt and California systems. In the Canary current however, upwelling favourable winds tend to weaken in some regions. Importantly, there is a strong agreement that significant trends in upwelling intensifications are evident at higher latitudes for all EBUS (Alves. and Miranda, 2013; Barton et al., 2013; Stocker et al., 2013). Of all EBUS, the most information on this subject is available from the California Current. In the central-northern portion of this system, upwelling winds primarily occur during the warm months of the year, while the seasonal range of pressure gradients in the southern portion of the system is reduced, and upwelling can occur there year-round. Overtime, the timing of upwelling has trended toward later and shorter upwelling seasons in the northern portion of the California System and longer upwelling seasons in the southern portion (Bograd et al., 2009). In contrast, a modelling study on wind stress curl found increased upwelling in the late season in the northern California System (Diffenbaugh et al., 2004).

The changes in trends derived from models may be due to their coarse resolution, which does not adequately represent smaller scale coastal processes such as upwelling (Caabella et al., 2014). Alternatively, this might be due to failing to adequately incorporate factors such as cloud cover or land-ocean pressure gradients which are useful to identify upwelling. Downscaling global models to the coastal domain of EBUS is required to address some of these issues. When incorporating these factors in studies, promising results are obtained (Garreaud and Falvey, 2009).

There is substantial but conflicting evidence on SST trends in EBUS (Rimbu et al., 2003; Belkin, 2009; Garcia-Reyes and Largier 2010). This is because spatio-temporal resolutions of SST capturing various aspects of upwelling processes and trends are unclear by the interannual to multi-decadal variability that result from oceanographic and atmospheric processes (Snyder et al., 2003). Different SST of differing resolutions suggest different trends within EBUS (Rimbu et al., 2003). The coarse resolution of SST datasets often makes it extremely difficult to separate nearshore upwelling related temperatures from regional and EBUS temperatures. These data products are also unable to solve small scale advection or retention within these systems which ultimately show different trends. Lima and Wethey (2012) use high resolution data to show cooling trends for coastal areas in all but the Canary upwelling system. A consistent agreement along all research is that coastal and offshore temperature trends differ. These studies show increasing or decreasing trends in the nearshore SST, compared with increasing trends in the Benguela (Rouault et al., 2010; Santos et al., 2012) and California upwelling systems (Mote and Salathé, 2010). These trends match the trends of increasing upwelling favourable winds (Sydeman et al., 2014). Climate change associated trends in EBUS may be uncertain by the effects of inshore cooling and offshore warming.

The Humboldt Current System is found to be the only EBUS whose SST trends shows a consistent negative linear trend over a time series of 36 years (Baumann and Doherty, 2013; Seabra et al., 2019). The Aguirre et al. (2019) reanalysis of an ensemble of GCMs found increases in summertime upwelling-favourable winds for both the Benguela current system (BCS) and Canary current system (CnCS). For the CnCS. Rykaczewski et al. (2015) found that a majority of models project significant increases in summertime intensity of upwelling; however, both Wang et al. (2015) and Rykaczewski et al. (2015) detected weakening in upwelling for the lowest latitudes of the CnCS.

1.2.4. Climate Change

Climate change as a result of anthropogenic warming is a global concern of both scientific and political importance. As the human population grows, the rate of global warming increases, resulting in profound effects on marine and other ecosystems (Stenseth et al., 2002; Harley et al., 2006; Hoegh-Guldberg and Bruno, 2010). Climbing temperatures cause a host of additional changes to marine systems, such as rising sea levels, increased ocean stratification, decreased sea-ice extent, and altered patterns of ocean circulation and precipitation (Doney et al., 2011). As this warming intensifies, pressure gradients between land and sea increases, resulting in a greater intensity of upwelling winds (Bakun, 1990; 2010; 2015). In rare cases, projected upwelling increases may overcome the countervailing effects of upper-ocean warming and stratification to cause regional cooling (Auad et al., 2006). Mead et al. (2013) found that coastal ecosystems are at high risk as a result of climate change. More recently, Whitfield et al. (2016) confirmed that coastal biodiversity has been observed to be affected by these effects.

While EBUS have long been on the minds of researchers, their reaction to climate change was not completely questioned until 1990 when Andrew Bakun, published his seemingly simple, yet polemic hypothesis (Sydeman et al., 2014; Bakun et al., 2015). Although Bakun (1990) did not explicitly conclude that the primary productivity of these regions will increase with climate change, it is well understood that the livelihood of pelagic fish is linked to upwelling trends; therefore, in addition to predicting an increase in the rate of upwelling, the Bakun Hypothesis has been extended to postulations that envisage direct benefits for EBUS fisheries (Bakun, 2015).

1.2.5. The Bakun Hypothesis

The atmospheric and oceanic mechanisms responsible for upwelling are interdependent and a change in one variable such as wind direction can have an effect on the distantly related variables. Over the past three decades, the earth's atmospheric temperature has warmed by 1.2°C (Wycech et al., 2020) and the earth's oceans have warmed by approximately 0.6°C. Although both land and sea surface temperatures are expected to increase, the land's lower heat capacity will cause it to warm more rapidly than the earth's ocean (Huyer, 1983; Samantha et al., 2019; Zhang et al., 2019; Jakoboski et al., 2020). These differing heat capacities have led to an overall increase in the pressure gradient force occurring between land and sea. Implications of the pressure gradient force directly increase the equatorial wind speeds. As wind speeds accelerate, the rate of Ekman transport increases resulting in a larger amount of surface waters transferred offshore (Huyer, 1983). When coastal surface waters are displaced faster, the rate of coastal upwelling increases (Bakun et al., 2015). Given this, Bakun et al. (2010) proposed that if there was an increase in greenhouse gases, it would cause more heating during the day and more cooling during the night causing the temperature gradient to increase resulting in a strong pressure gradient, ultimately affecting wind patterns and therefore upwelling, imposing uncertainty in future upwelling trends (Bakun et al., 1990).

The hypothesis remains debated throughout the oceanographic community. Some researchers deny the logic behind this hypothesis and claim that EBUS warm faster than their neighbouring oceans, thus intensifying pre-existing land-sea pressure gradients. However, researchers also question whether the impact of differential heating has on pressure gradient force ultimately drives the intensification of upwelling within these regions (Rykaczewski et al., 2015; Brady et al., 2017). Rykaczewski et al. (2015) suggests that the mechanisms responsible for the intensification of upwelling dependent pressure gradient force is not driven by differential warming but rather intensifications are constrained to the poleward boundaries of the system and its upwelling season.

1.3. Extreme events in the context of upwelling

Extreme events such as marine heatwaves as defined by Hobday et al. (2016) are prolonged discrete anomalously warm water events that can be described by various statistical metrics such as intensity, duration and the count of events within a time series irrespective of its geographical location. Schlegel and Smit (2018) developed an algorithm that detects extreme events within long-term (> 30 years) daily time series of SST. It does so by finding the occasions when SST exceeds a threshold (the 90th percentile) in the probability distribution of the data based on an 11-day wide moving mean smoother centred on each day-of-the-year at each pixel. Similarly, upwelling signals could be detected in the same way by identifying a threshold when drops in temperature occur and by considering wind patterns as well as duration in order to classify an upwelling signal. Metrics of these upwelling signals could then be compared over a long time series to test for upwelling trends.

1.4. Rationale

Coastal upwelling impacts local climates and ecosystems by lowering atmospheric surface temperatures and this influencing wind patterns. While the width of upwelling bands only extends 10-30 km, their productive band extends to approximately 100 km. Hence, coastal upwelling serves as a host of nutrients for phytoplankton (Send et al., 1987), creating a region of survival and prosperity for small pelagic fish (Carr, 2001). Given the importance of coastal upwelling; understanding upwelling trends over time and finding an accurate way of identifying upwelling signals are important. By using the extreme event algorithm, we were able to identify signals to date, duration and intensity.

Since EBUS are responsible for over 17% of global fish catch, their response to climate change has become of particular interest to oceanographers and climatologists (Carr, 2001). During summer months, coastal winds are strengthened by the land based thermal low-pressure system, generally located east of permanent but seasonally migrating oceanic high pressure systems (Huyer, 1983; Seager et al., 2003; Montecino and Lange, 2009), with the biological productivity in EBUS being mainly as a result of warm seasonal upwelling, this study is important to test for variation in the duration, frequency and intensity of upwelling specifically during summer months.

1.4.1. Predictions/Hypotheses

We predict that intensified upwelling-favourable winds would lead to an increased upwelling rate and duration of these signals. Increased upwelling rates have significant effects on the surrounding ecosystems and fisheries (Bakun 1990, Bakun et al., 2010). As such, it is important to monitor upwelling trends during the most predominant upwelling period. The importance of coastal upwelling systems is widely recognised but their behaviour is still uncertain (Bakun et al.,

2010). Here we hypothesize that upwelling detected at the coastline (0 km) may not be the same signal detected at a distance of 50 km from the coastline given the differences in resolution of SST remotely sensed data. It is also predicted that a higher resolution SST data would likely detect an upwelling signal compared to coarse resolution data. It may therefore be assumed that human responses to poor upwelling detections and changes in upwelling trends as a result of climate change will negatively influence these productive zones. In order to investigate upwelling trends, the detection and collection of SSTs, wind speed, and wind direction data are important. The method used to detect upwelling will represent an extensive body of work and so the application of these results to biotic factors will not be accomplished extensively in this thesis. The important knowledge obtained by this research will branch out into different fields of study, with this it is critical that the work done within this thesis is accessible to other research groups.

CHAPTER 2

UPWELLING SIGNALS: A COMPARISON OF SEA SURFACE TEMPERATURE IN THE BENGUELA

Abstract

The importance of coastal upwelling systems is widely recognised. However, several aspects of the current and future behaviours of these systems remain uncertain. Fluctuations in temperature as a consequence of anthropogenic climate change are hypothesised to affect upwelling-favourable winds and coastal upwelling is expected to intensify across all Eastern Boundary Upwelling Systems. In this paper we used sea surface temperature data from five different products of varying resolutions, in conjunction with wind data, to detect and analyse upwelling signals at four sites within the Benguela Upwelling System at varying distances from the coastline. We found that upwelling signals were not uniformly detected across the five products for each of the four sites and that the durations of those signals were longer when using SST data products with higher spatial resolutions. Moreover, the high-resolution data products were significantly more likely to display upwelling signals at a distance of 25 km away from the coastline when signals were also detected at shoreline. Our findings promote the viability of SST and wind time series data towards detecting and predicting upwelling signals within coastal upwelling systems. However, our results also highlight the importance of high-resolution data products to improve the accuracy of such estimates. This study represents an important step towards the development of a novel method for predicting the behaviours of coastal upwelling systems.

Keywords: Seawater temperature, coastal regions, code: R, upwelling

2.1. Introduction

Sea surface temperature (SST) is regarded as one of the most important variables in the coupled ocean-atmosphere systems, and is a particularly useful research tool in the scientific fields of meteorology and oceanography (Mesias et al., 2007; Harlass et al., 2015). For over 150 years, SST data have been collected using *in situ* measurement techniques (Rayner et al., 2003) with satellite measurements of SST being available since the 1970s (Reynolds et al., 2013). Over the past decade, techniques have been developed to allow the assimilation and blending of different SST datasets from various *in situ* and satellite platforms. These are referred to as the Level-3 and Level-4 high resolution gap-free products. Previous studies demonstrated that satellite-based SST data are less accurate than *in situ* data due to the complexity of the oceanic and atmospheric conditions that need to be accounted for in deriving satellite SST products (Robinson et al., 1984; Brown et al., 1985; Minnett, 1991; Smit et al., 2013). The reason for this is that the sensors only 'look' at a restricted portion of the ocean for several minutes at a time; the exception being of-course, geo-stationary satellites like the POES (polar orbiting environmental satellite). These errors vary both regionally and temporally (Wick et al., 1992). In comparison to *in situ* SST measurements collected from ships or buoys, a major advantage of satellite SST is their global coverage and near real time availability. SST datasets with a high level of accuracy, spatial completeness, and fine-scale resolution are necessary for weather and climate forecasting and are of great importance for reliable climate change monitoring (Reynolds and Smith, 1995; Smith et al., 1998; Reynolds and Smith, 2002; Chao et al., 2009).

Long-term SST data have been obtained from two kinds of satellite remote sensors. Thermal infrared (TIR) and microwave (MW) sensors have different weather sensitivity characteristics and accuracies (Li et al., 2013). TIR SST products are available from the 1970s and may have a spatial resolution as fine as approximately a 4 km grid; however, they are affected by the presence of clouds and other aerosols in the atmosphere, which is known to result in spatial discontinuity. MW SST products have a lower resolution than TIR SSTs at approximately a 25 km grid, leading to a much lower accuracy near coastlines (Parinussa et al., 2008; Li et al., 2013). By combining these different types of SST products, it is possible to take advantage of the strengths within both, and each sensor type can help produce an SST dataset with more spatial and temporal coverage and higher resolution.

For many applications, SST data are not used or provided at the full resolution of the sensors, but are averaged over defined areas in order to produce a gridded product (Reynolds et al., 2002; Bulgin et al., 2016). Gridding in this way destroys more detailed information and as a result a gridded SST measurement is taken as an estimate of the average SST across a specific grid cell over a certain time period. Spatial sampling uncertainty and temporal averaging is present in gridded products as the full gridded cell is often not being observed as a result of interference due to the presence of clouds or aerosols, as previously mentioned. In existing daily global SST analysis products, typical grid resolution ranges from 0.05° × 0.05° to 0.25° × 0.25°, or from approximately 5 to 25 km (e.g., Reynolds and Smith, 1994; Brasnett, 2008; Donlon et al., 2012). Small-scale features can evolve during the course of the day, but the sensor sampling during this time is not dense enough for the sub-daily global analyses at a high spatial resolution (Reynolds and Chelton, 2010; Reynolds et al., 2013). Furthermore, considering that the satellites are passing overhead only once every ~24 hours, images are only captured at very specific times during the day. To capture these small-scale features in a gridded analysis, it is suggested that the development of an improved analysis would have high resolution at small-scale features in regions of good coverage and lower resolution in areas of poor coverage (Reynolds et al., 2013).

In order to assess the suitability of a range of SST products for the detection of upwelling signals, this study aimed to observe patterns and trends in upwelling signals in the Benguela upwelling system (BUS) across a range of localities and spatial scales off the South African West Coast. We selected an upwelling system for this study because this physical process provides a strong signal of increasing and decreasing SST that is strongly localised to known centres of upwelling, and which relates to the coastal wind field that drives the offshore advection of water mass. Here, a unique method for identifying upwelling signals was used. This method made use of wind variables as seen in Fielding and Davis (1989), but also applied a novel upwelling signal detection method to SST, which allowed for a more accurate identification of upwelling. Because upwelling is such a well characterised oceanographic process, the resultant fluctuating SST signal should be observed across independent SST products. Here we assess blended SST products covering a range of spatial grid resolutions from 0.05° × 0.05° to 0.25° × 0.25°. We hypothesised that the higher resolution data should have a better fidelity at detecting these upwelling signals, some of which might only be confined to smaller spatial scales or localised closer to the shore.

The BUS is one of the four major Eastern Boundary Upwelling Systems (EBUS) (Bakun et al., 2015). EBUS are characterised as vast regions of coastal ocean occurring along the western shores of continents bordering the Pacific and Atlantic Oceans (Bakun, 1990; Pauly and Christensen, 1995; Bakun et al., 2010; Bakun et al., 2015). Coastal upwelling associated with EBUS is known to have a large influence on the associated ecosystem's primary productivity, and hence the abundance, diversity, distribution and production of marine organisms at all trophic levels (Bakun et al., 2010;

2015). The upwelling process is also hypothesised to be strongly affected by anthropogenic climate change. According to the 'Bakun hypothesis,' an increase in greenhouse gases will result in an increase in day-time warming and night-time cooling and ultimately cause an increase in temperature gradients which will form stronger atmospheric pressure gradients (Bakun, 1990). These pressure gradients modulate the winds which ultimately affect the intensity and duration of upwelling (Hsieh and Boer, 1992; Mote and Mantua, 2002; Bakun et al., 2010; Lima and Wethey, 2012). Concrete evidence in support of Bakun's hypothesis is not yet available (see Chapter 3)—I think in part because of the difficulties associated with identifying the upwelling signals themselves. I anticipate that the work outlined in this chapter will make a valuable contribution in this regard, and to this this end I will apply the learning emerging here to Chapter 3, where trends in upwelling dynamics will be assessed for the world's four major EBUS. Since changes in SST indirectly affect coastal communities, and have considerable, often far-reaching economic impacts (Murawski, 1993; Bakun et al., 2010), this work could be of great importance to our understanding of how climatic change might affect EBUS in decades to come.

2.2. Methods

2.2.1. Site Selection

The western region of the South African coastline is dominated by the Benguela Current, which forms the foundation of an Eastern Boundary Upwelling System (EBUS) (Hutchings et al., 2009), and it provides a natural laboratory for this study. Annual mean coastal seawater temperatures within this region have a range of 12.3 ± 1.2°C at the western limit near the Namibian border. Seasonal upwelling is controlled by south-easterly trade winds, with intense upwelling occurring throughout the summer months. This creates distinct temperature variations with much lower temperatures within the upwelling cells over a fairly narrow continental shelf found from the Cape Peninsula to Cape Columbine. In order to examine upwelling patterns at different distances from the coastline within the southern Benguela region, several sites from the SACTN dataset (Schlegel and Smit, 2016; Schlegel et al., 2017) along the west coast of South Africa were selected. The main objective of this study was to identify upwelling signals with a variety of data products. This involved four separate SST products that covered a time period of four years. To assess upwelling metrics within the BUS four sites were selected as points of comparison. Each site was situated along the West Coast of South Africa at various distances from the upwelling centre of the BUS (**Figure 2.1**).

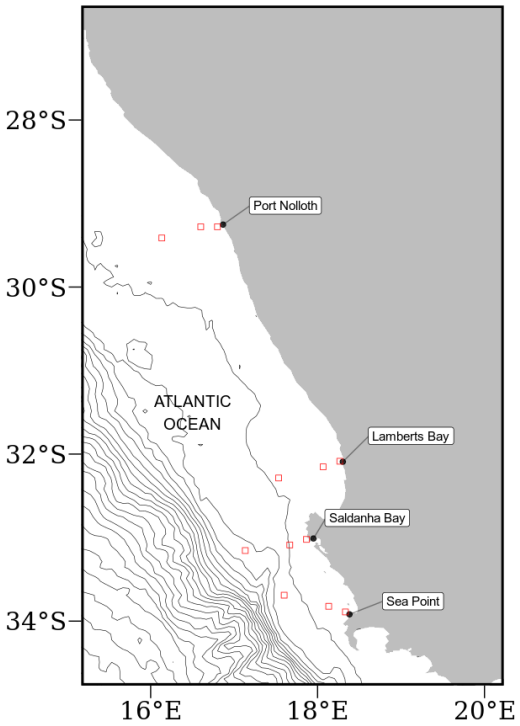

Figure 2.1: Map of southern Africa showing and coastal bathymetry. The black points represent the location of the *in situ* temperature sites and the empty red boxes show the pixels used along the shore normal transect from the satellite sea surface temperatures (SST) time series. The red boxes are at 0 km, 25 km and 50 km from the coastline.

2.2.2 Datasets

This study uses four Level-4 remotely sensed temperature datasets compiled by a number of organisations. The AVHRR-only (Advanced Very High-Resolution Radiometer) Optimally-Interpolated Sea Surface Temperature (OISST) dataset has been providing global SSTs for nearly four decades (Reynolds and Smith, 1994). OISST is a global 0.25° × 0.25° gridded daily SST product that assimilates both remotely sensed and *in situ* sources of data to create a gap free product (Banzon et al., 2016). The version 3.0 Group for High Resolution Sea Surface Temperature (GHRSST) product has a 0.2° × 0.2° global grid resolution and is constructed by the Canadian Meteorological Center (CMC). It combines infrared satellite SST at numerous points in the time series from the AVHRR, the European Meteorological Operational-A (METOP-A) and Operational-B (METOP-B) platforms, as well as the microwave SST data from the Advanced Microwave Scanning Radiometer 2 in conjunction with *in situ* observations of SST from ships and buoys from the ICOADS program. The Multi-scale Ultra-high Resolution (MUR) SST Analysis is produced using satellite instruments with datasets spanning 1 June 2002 to present times. MUR provides SST data at a spatial resolution of 0.01° × 0.01° and is currently among the highest resolution SST datasets available. The final dataset used is the GHRSST analysis produced daily using a multi-scale two-dimensional variational (MS-2DVAR) blending algorithm on a global 0.01° grid known as G1SST. This product uses satellite data from a variety of sensors, such as AVHRR, the Advanced Along Track Scanning Radiometer (AATSR), the Spinning Enhanced Visible and Infrared Imager (SEVIRI), the Moderate Resolution Imaging Spectroradiometer (MODIS), and *in situ* data from drifting and moored buoys. We see that not all products are completely independent as they share the use of AVHRR SST data, but the amount of subsequent blending, the incorporation of other SST data sources, the different blending and interpolation approaches used, and the differing final grid resolutions make them acceptably different for this study.

Additionally, this study uses the South African Coastal Temperature Network (SACTN) dataset for its *in situ* temperature records. This dataset consists of coastal seawater temperatures obtained from 129 sites along the South African coastline, measured daily from 1972 until 2017 (Schlegel and Smit, 2016; Schlegel et al., 2017). Of these, 80 were measured using hand-held thermometers and the remaining 45 were measured using underwater temperature recorders (UTRs). For this analysis, the data were combined and formatted into standardized comma separated values (CSV) files which allowed for a fixed methodology to be used across the entire dataset.

An advantage to using *in situ* data over satellite data is that they may provide a more accurate representation of the thermal properties closer to the coast, whereas satellite data often fail to accurately capture and represent temperature properties within the same spatial context. The result is that *in situ* data can more accurately explain upwelling signals within the coastal inshore environment. Further, evidence by Smit et al. (2013) has shown that satellite data along the South African coastline may have a warm bias as high as 6 °C greater than *in situ* temperatures within the nearshore environment. In order to create a time series of each of the remotely sensed SST data products, shore-normal transects of all Level-4 products were extended at west coast stations where the *in-situ* data in the SACTN database were available. Time series of SSTs were extracted at 0, 25 and 50 km along these shore-normal transects from the coast **Figure 2.1**.

2.2.3 Wind data

Wind data were obtained from the South African Weather Service (SAWS), and were provided at three-hour resolutions. Specific wind characteristics were measured, namely, wind direction (dirw) and wind speed (spw). Wind was an important variable for this study as wind direction and wind speed have a direct influence on the intensity and duration of upwelling, consequently, wind data collected from 1989-01-01 to present were investigated for their relationship with upwelling at the sites for which SST time series were extracted.

2.2.4 Defining and determining upwelling

In order to detect and analyse upwelling signals at four sites within the BUS, it was first necessary to define when upwelling was occurring; however, to accomplish this a set of threshold values for identifying when the phenomenon was taking place was required. Given that upwelling is primarily caused by alongshore, equatorward winds, both SST and wind data were used. The wind data were used to inform an upwelling index calculated using the formula presented in the work by Fielding and Davis (1989):

$$upwelling\ index = \mu(\cos\theta - 160)$$

where μ represents the wind speed (m/s), θ represents the wind direction in degrees, and 160 is the orientation of the west coast (Jury 1980). The index relies heavily on wind speed and direction data in order to identify the presence and intensity of upwelling. The above equation produces a value called the upwelling index. An upwelling index < 0 represents downwelling whilst an upwelling index > 0 represents upwelling (Fielding and Davis, 1989). When the upwelling index is greater than 0, SSTs usually drop, as expected, suggesting that upwelling is occurring. It was found that the drop in SST that coincided with a positive upwelling index was close to the seasonally varying 25th percentile threshold for SST, so this threshold temperature was used in combination with the upwelling index to identify when upwelling may be occurring. With the threshold set for which temperatures may qualify as an upwelling signal it was then necessary to identify the number of consecutive days that must be exceeded for an upwelling signal to qualify as a discrete event. Here it must be noted that upwelling is known to vary on a seasonal basis and may also occur hourly (sub-daily). Therefore, the minimum duration for the classification of an upwelling signal was set as one day, the rationale being that data from the SACTN dataset as well as the satellite remotely sensed SST data are collected only at a daily resolution, preventing a temporally finer definition. With the upwelling index, temperature threshold, and duration for an upwelling signal established, the detect_event() function from the **heatwaveR** package (Schlegel and Smit, 2018) was used to calculate metrics for the upwelling signals. Because upwelling signals were calculated relative to percentile exceedances, rather than an absolute definition such as temperatures below a fixed temperature threshold, upwelling signals could occur any time of the year; however, upwelling was shown to be more dominant summer months (December, January and February), as expected. This method of determining upwelling signals is unique as it considers both SST and wind pattern, and provides us with a descriptive statistical output of each of the signals detected (**Table 2.1**).

Table 2.1: Metrics of upwelling signals and their descriptions.

Name [unit]	Definition
Duration [days]	Consecutive period of time that temperature exceeds the threshold
Mean intensity [°C]	Highest temperature anomaly value during the signal
Cumulative intensity [°C.days]	Sum of the daily intensity anomalies over a duration of the event

ANOVAs were used to compare the upwelling metrics such as duration, intensity, and cumulative intensity against the main effects: *site*, *product* and *distance*. Upwelling metrics as a function of satellite product type was assessed using *product* as main effect, and nesting *distance* within *site*. To establish whether differences existed between sites or distances from the shore, the upwelling metrics were assessed as a function of *site* or *distance*, independently for each satellite. Restrictions to experimental design prevented testing interaction effects within *product* types. In the analysis the relationship between the SST products across the various selected study sites were established; factors used to correlate these relationships included duration and the number of signals detected. These analyses sought to test if significant differences occurred between sites and data products. A Pearson Product Moment correlation was used to identify if the same upwelling signal detected at a distance of 0 km from the coastline would be visible at a distance of 25 km from the coastline and similarly if the same upwelling signal could be observed when comparing at a distance of 0 and 50 km from the shore. The signals were classified by start and end date and within the same data product. Thereafter, the average numbers of upwelling signals detected by each individual data product across all sites were compared using an ANOVA test.

2.3. Results

A one-way ANOVA indicated no significant difference in upwelling duration between sites within the South African portion of the BUS as detected in the CMC (d.f. = 3, $F = 0.88$, $p > 0.05$) and OISST (d.f. = 3, $F = 0.76$, $p > 0.05$) (**Table 2.2**, **Figure 2.2**) products. However, a significant difference was found between the G1SST (d.f. = 3, $F = 3.46$, $p < 0.05$), MUR (d.f. = 3, $F = 4.45$, $p < 0.005$) and SACTN (d.f. = 3, $F = 3.61$, $p < 0.01$) data products. The Sea Point site had the longest mean duration of upwelling signals detected. Lamberts Bay and Port Nolloth had the shortest duration of upwelling signals detected. Particularly, Lamberts Bay in the SACTN data product yield the shortest duration of upwelling signals.

A significant difference was found in upwelling mean intensity between sites in the CMC (d.f. = 3, $F = 5.29$, $p < 0.001$), OISST (d.f. = 3, $F = 7.56$, $p < 0.001$) and SACTN (d.f. = 3, $F = 17.82$, $p < 0.001$) products. However, no significant difference was found in the G1SST (d.f. = 3, $F = 2.01$, $p > 0.05$) and MUR (d.f. = 3, $F = 1.38$, $p < 0.05$) products (**Table 2.3**, **Figure 2.3**). Sea Point represents the highest mean intensity of upwelling signals collected among all of the remotely sensed SST. Differences in means were present across data products at each site individually but were consistent across sites (i.e. each data product detected a similar means at each of the respective sites.

Table 2.2: One-way ANOVA evaluating the variation in the duration of upwelling signals detected in the various gridded SST and in situ products between four sites within the Benguela Current region of South Africa. Comparisons are graphically captured in **Figure 2.2**.

Data product		d.f.	M.S.	*F*-value	*P*-value
CMC	site	3	21.68	0.88	> 0.05
	residuals	132	24.52		
G1SST	site	3	158.99	3.46	< 0.05
	residuals	268	45.93		
MUR	site	3	445.1	4.45	< 0.005
	residuals	155	100.1		
OISST	site	3	68.13	0.76	> 0.05
	residuals	169	8895		
SACTN	site	3	24.84	3.61	< 0.01
	residuals	280	7.156		

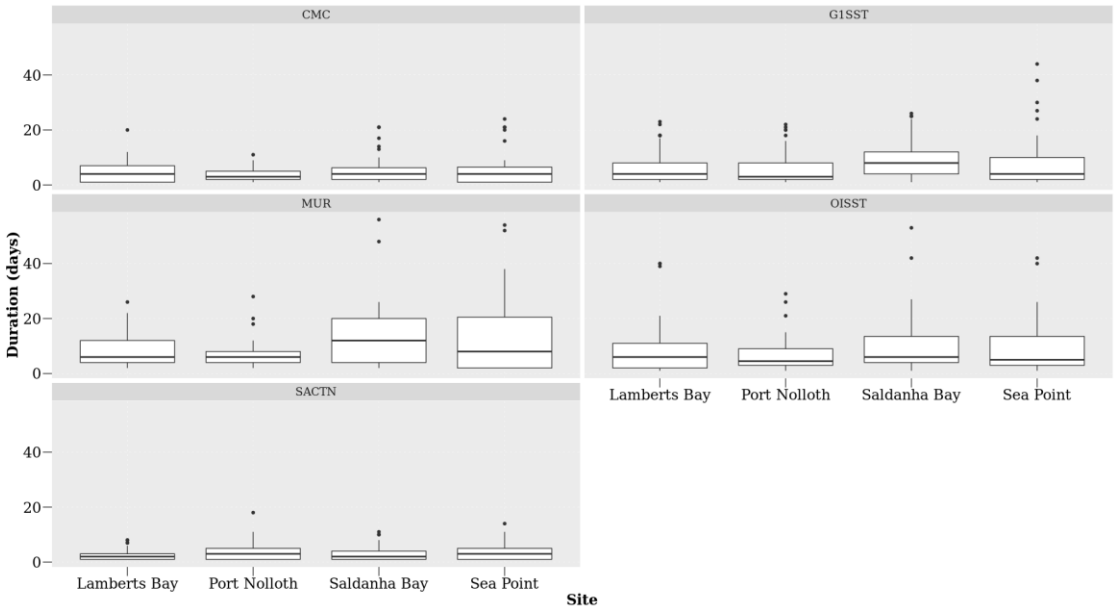

Figure 2.2: The upwelling duration for each of the signals detected for the four satellite products and the SACTN *in situ* collected data during summer months (December, January and February), over a four-year period.

Table 2.3: One-way ANOVA evaluating the variation in the mean intensity of upwelling signals detected in the four gridded SST and *in situ* products between the four sites within the Benguela Current region of South Africa. Comparisons are graphically captured in **Figure 2.3**.

Data product		d.f.	M.S.	*F*-value	*P*-value
CMC	site	3	0.56	5.29	< 0.001
	residuals	132	0.11		
G1SST	site	3	0.67	2.01	> 0.05
	residuals	268	0.34		
MUR	site	3	0.42	1.38	> 0.05
	residuals	155	0.31		
OISST	site	3	1.76	7.56	< 0.001
	residuals	168	0.23		
SACTN	site	3	5.29	17.82	< 0.001
	residuals	280	0.29		

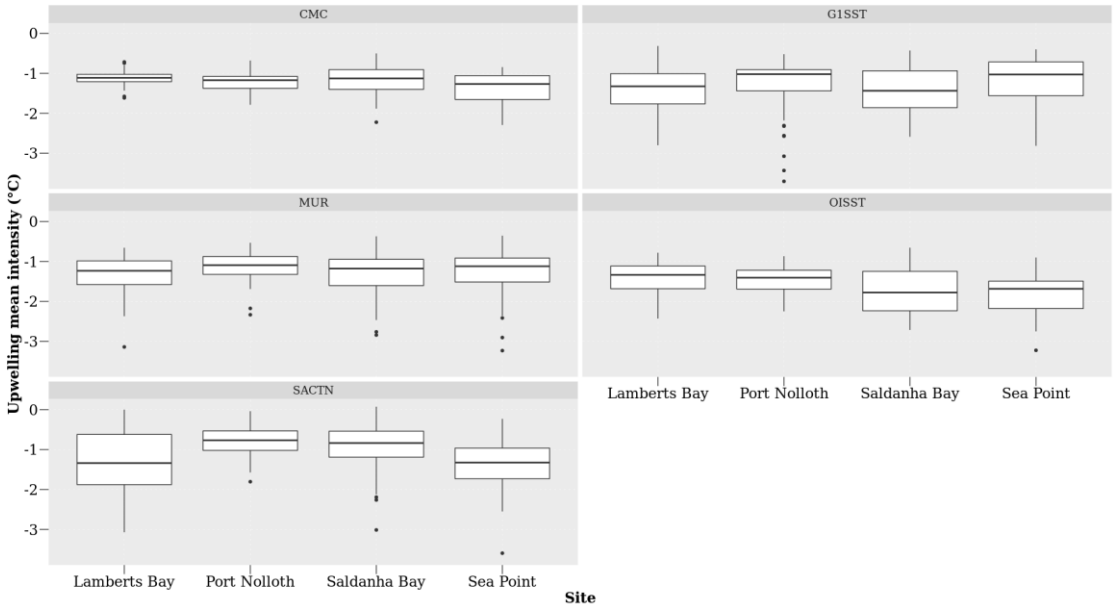

Figure 2.3: The mean intensity for each of the signals detected for the four satellite products and the SACTN *in situ* collected data during summer months (December, January and February), over a four-year period.

Table 2.4: One-way ANOVA evaluating the variation in upwelling cumulative intensity as detected in the four gridded SST and *in situ* products between four sites within the Benguela Current region of South Africa. Comparisons are graphically captured in **Figure 2.4**.

Data product		**d.f.**	**M.S.**	***F*-value**	***P*-value**
CMC	site	3	64.43	1.23	> 0.05
	residuals	132	52.25		
G1SST	site	3	500.9	2.96	< 0.05
	residuals	268	169.2		
MUR	site	3	2317.6	3.81	< 0.01
	residuals	155	609.5		
OISST	site	3	744.7	1.54	> 0.05
	residuals	169	484.8		
SACTN	site	3	122.53	9.44	< 0.0005
	residuals	280	12.98		

There was no significant difference in upwelling cumulative intensity between sites within the South African portion of the BUS as detected in the CMC (d.f. = 3, $F = 1.23$, $p = 0.3$) and OISST (d.f. = 3, $F = 1.54$, $p > 0.05$) data product (**Table 2.4**, **Figure 2.4**). A significant difference in cumulative intensity of upwelling signals was found in the G1SST (d.f. = 3, $F = 2.96$, $p < 0.05$), MUR (d.f. = 3, $F = 3.81$, $p < 0.01$) and SACTN (d.f. = 3, $F = 9.44$, $p < 0.001$) data products during the summer season. The cumulative intensity of upwelling signals is most intense in Saldanha Bay and Sea Point for the MUR, G1SST and OISST products. The cumulative intensity from sites within the SACTN data product were the lowest.

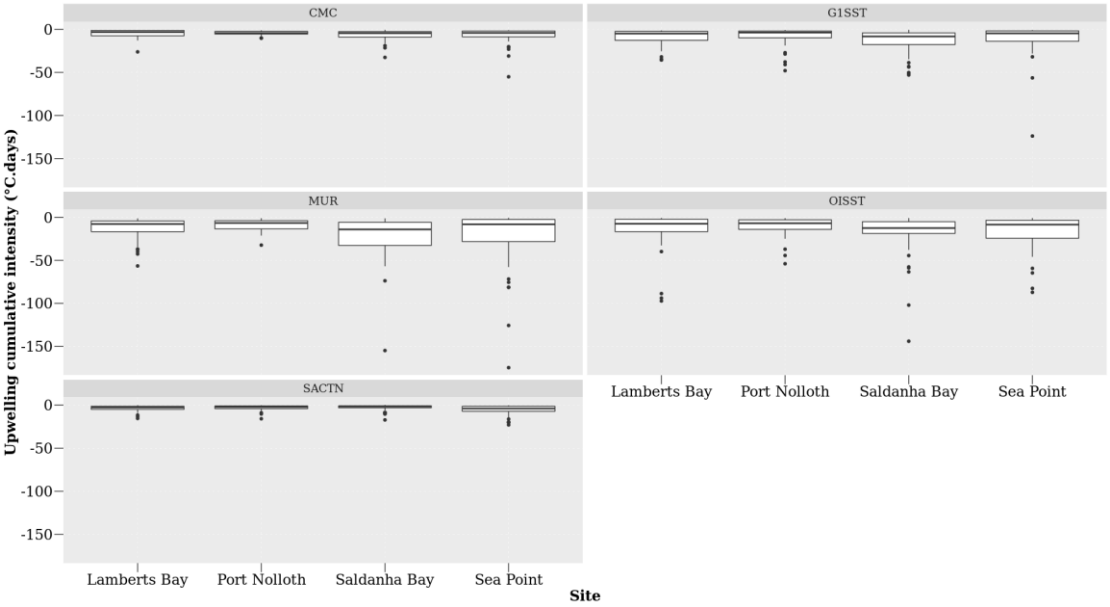

Figure 2.4: The upwelling cumulative intensity for each of the signals detected for the four satellite products and the SACTN *in situ* collected data during summer months (December, January and February), over a four-year period.

An ANOVA showed that no significant difference exist in the duration of upwelling signals detected at different distances from the shore during the summer season in the CMC (d.f. = 2, $F = 0.86$, $p > 0.04$), G1SST (d.f. = 2, $F = 0.59$, $p > 0.05$), MUR (d.f. = 2, $F = 2.29$, $p > 0.05$) and OISST data (d.f. = 2, $F = 1.61$, $p > 0.05$) products. The MUR and G1SST often detected the longest duration of upwelling signals at a distance of 0 and 25 km from the shore (**Table 2.5**, **Figure 2.5**).

Table 2.5: One-way ANOVA evaluating the variation in the duration of upwelling signals detected at the various distances from the shore for the four gridded SST product between at the various distances from the shore. Comparisons are graphically captured in **Figure 2.5**.

Data product		d.f.	M.S.	*F*-value	*P*-value
CMC	distance	2	21.15	0.86	> 0.05
	residuals	133	24.5		
G1SST	distance	2	27.81	0.59	> 0.05
	residuals	269	47.33		
MUR	distance	2	308	2.29	> 0.05
	residuals	156	104.1		
OISST	distance	2	141.31	1.61	> 0.05
	residuals	170	87.89		

Table 2.6: One-way ANOVA evaluating the variation in the mean intensity of upwelling signals detected in the four gridded SST product between at the various distances from the shore. Comparisons are graphically captured in **Figure 2.6**.

Data product		d.f.	M.S.	*F*-value	*P*-value
CMC	distance	2	0.32	2.89	< 0.05
	residuals	133	0.11		
G1SST	distance	2	7.36	25.71	< 0.001
	residuals	269	0.25		
MUR	distance	2	5.29	21.74	< 0.0001
	residuals	156	0.24		
OISST	distance	2	1.62	6.68	< 0.001
	residuals	170	0.14		

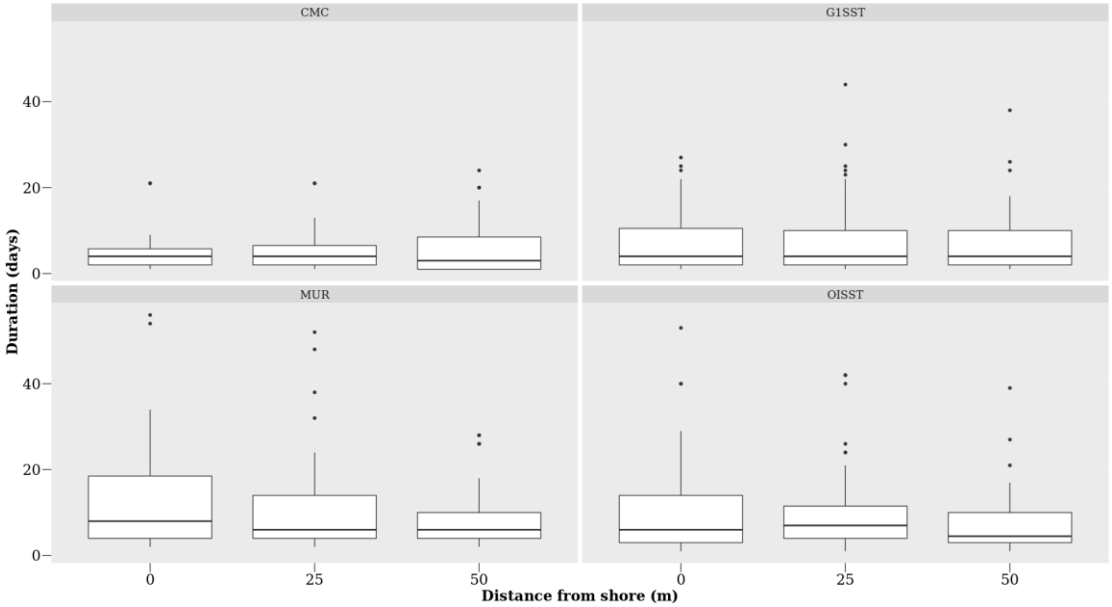

Figure 2.5: The duration for each of the signals detected at the various distances from the shore for the four satellite products during summer months (December, January and February), over a four-year period.

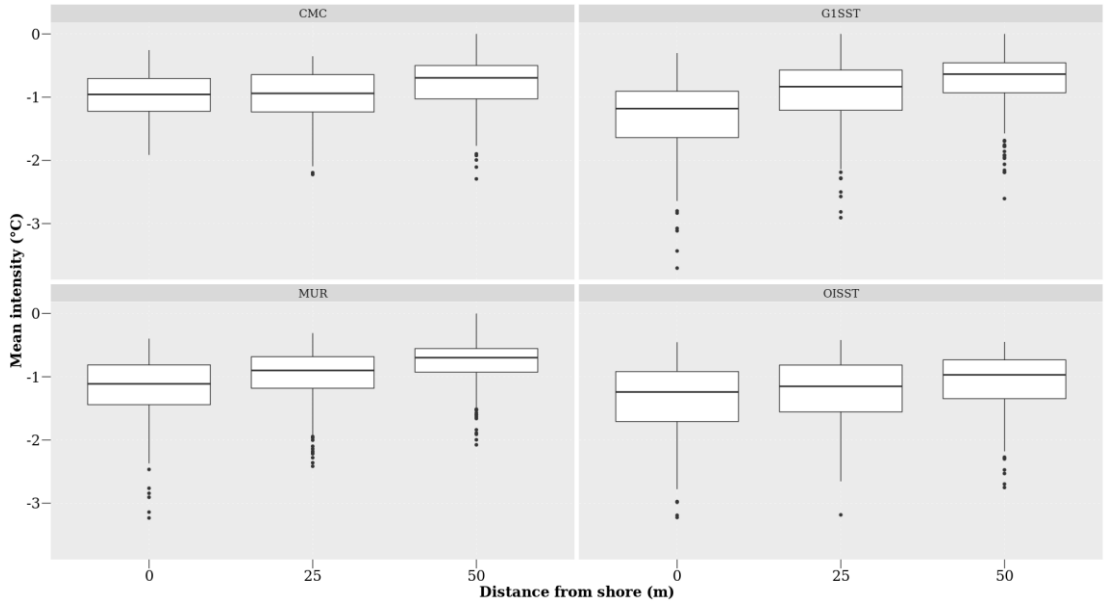

Figure 2.6: The mean intensity for each of the signals detected at the various distances from the shore for the four satellite products during summer months (December, January and February), over a four-year period.

Significant difference in the mean intensity of upwelling signals were detected at different distances in all of the remotely sensed SST products. CMC (d.f. = 2, $F = 2.89$, $p < 0.05$), G1SST (d.f. = 2, $F = 25.71$, $p < 0.001$), MUR (d.f = 2, $F = 21.74$, $p < 0.001$) and OISST (d.f. = 2, $F = 6.68$, $p < 0.001$). MUR and G1SST products recorded the highest mean intensity of upwelling signals at a distance of 0 km from the shore (**Table 2.6**, **Figure 2.6**). The mean intensity of upwelling decreased further away from the shore in all of the SST products.

Table 2.7: One-way ANOVA evaluating the variation in the cumulative intensity of upwelling signals at the various distances from the shore detected in the four gridded SST product between at the various distances from the shore. Comparisons are graphically captured in **Figure 2.7**.

Data product		d.f.	M.S.	*F*-value	*P*-value
CMC	distance	2	48.62	0.93	> 0.05
	residuals	133	52.58		
G1SST	distance	2	915.1	5.47	< 0.05
	residuals	269	167.4		
MUR	distance	2	3860	6.42	< 0.05
	residuals	156	601		
OISST	distance	2	1061.3	2.19	> 0.05
	residuals	170	482.6		

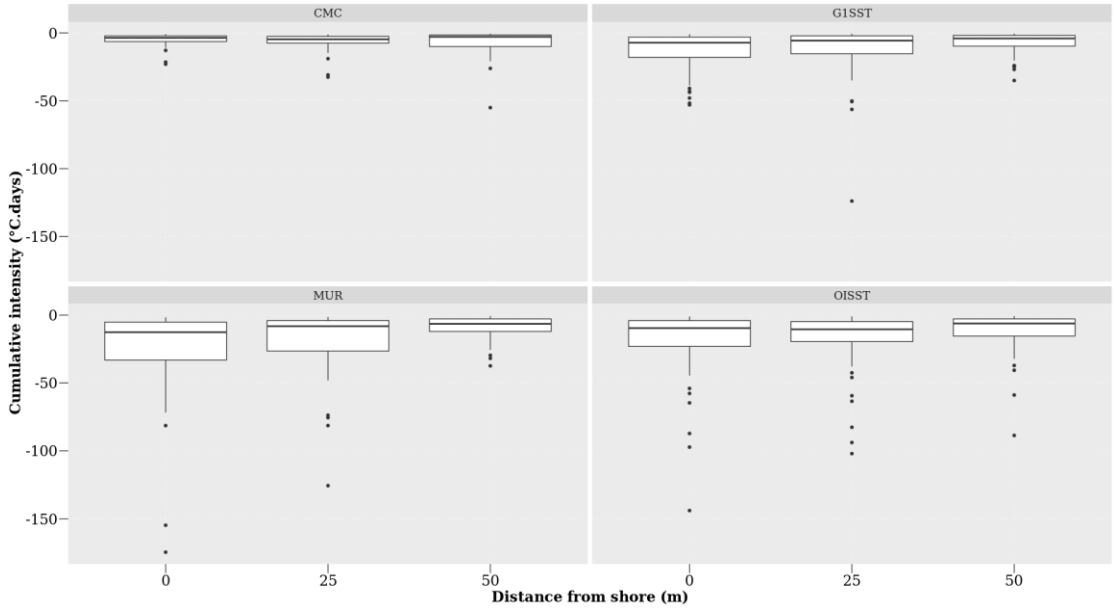

Figure 2.7: The cumulative intensity for each of the signals detected for the four satellite products during summer months (December, January and February), over a four-year period.

A one-way ANOVA showed a significant difference in the cumulative intensity of upwelling signals detected at different distances from the shore in the G1SST (d.f. = 2, $F = 5.46$, $p < 0.005$) and MUR (d.f. = 2, $F = 6.42$, $p < 0.005$) data products. (**Table 2.7**, **Figure 2.7**). However, the CMC (d.f. = 2, $F = 0.93$, $p > 0.05$) and OISST (d.f. = 2, $F = 2.19$, $p > 0.05$) products showed no significant difference in cumulative intensity of upwelling signals detected. The MUR and OISST product observed the highest cumulative intensity at a distance of 0 km from the coastline, this intensity decreases further away from the coastline. The cumulative intensity of upwelling signals for all product decreased further from the shore.

A nested ANOVA (**Table 2.8**, **Figure 2.8**) showed that there is a significant difference in the duration of upwelling signals detected amongst the data products (nested ANOVA, d.f. = 3, $F = 13.43$, $p < 0.001$). The MUR product had the longest duration of upwelling signals while the CMC products had the shortest.

Table 2.8: Nested ANOVA evaluating the variation in upwelling duration as detected in four gridded SST products (OISST, CMC, G1SST, and MUR) at several distances away from the shore and sites within the Benguela Current region of South Africa. Only the main effect due to 'product' is indicated. Comparisons are graphically captured in **Figure 2.8**.

	d.f.	**M.S.**	***F*-value**	***P-value***
Product	3	849.3	13.43	< 0.001
residuals	725	63.2		

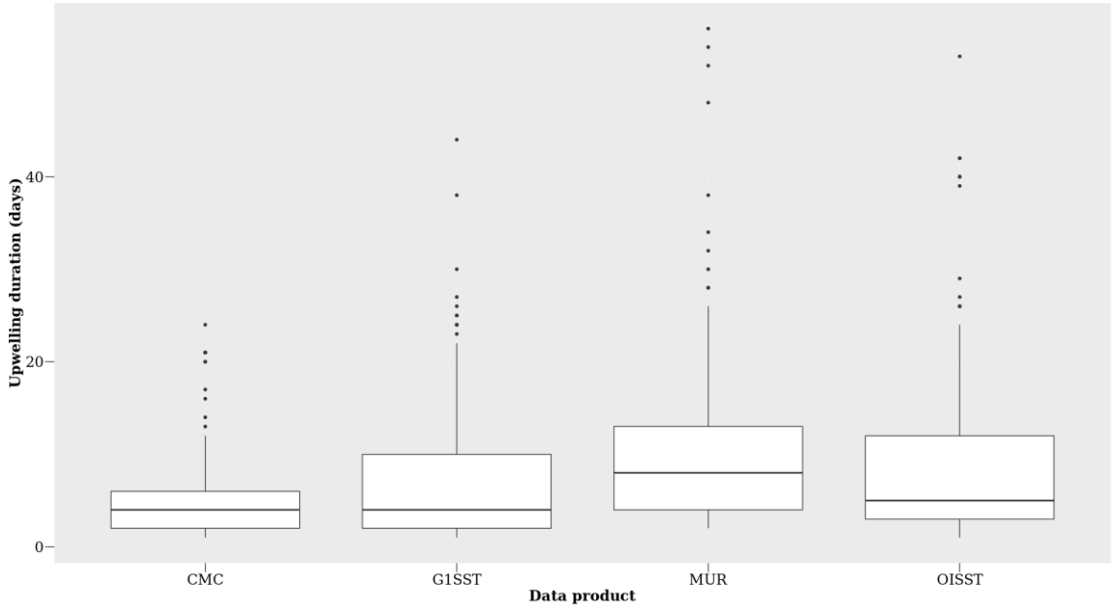

Figure 2.8: The duration of upwelling signals detected for the four satellite products at the different distances from the shore during summer months (December, January and February), over a four-year period.

Table 2.9: Nested ANOVA evaluating the variation in the mean intensity of upwelling signals are detected in four gridded SST products (OISST, CMC, G1SST, and MUR) at several distances away from the shore and sites within the Benguela Current region of South Africa. Only the main effect due to 'product' is indicated. Comparisons are graphically captured in **Figure 2.9**.

	d.f.	**M.S.**	***F*-value**	***P-value***
Product	3	4.45	19.84	< 0.001
residuals	725	0.22		

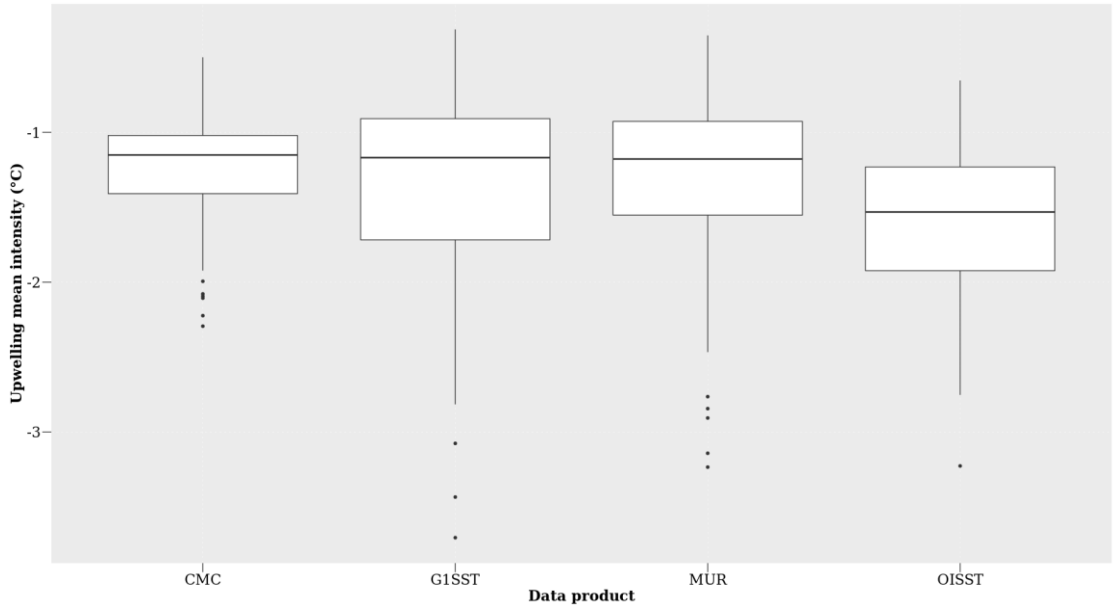

Figure 2.9: The mean intensity for each of the signals detected for the four satellite products at difference distances from the shore during summer months (December, January and February), over a four-year period.

The ANOVA analysis suggests (**Table 2.9**, **Figure 2.9**) that there is a significant difference in the mean intensity of upwelling signals detected between the data products of variable resolution (nested ANOVA, d.f. = 3, $F = 19.84$, $p < 0.001$). The G1SST and MUR data products represented the highest mean intensity while CMC represented the lowest mean intensity of upwelling signals.

I found (**Table 2.10**, **Figure 2.10**) that there is a significant difference in the cumulative intensity of upwelling signals detected between the data products of variable resolution (nested ANOVA, d.f. = 3, $F = 14.12$, $p < 0.001$). The MUR SST product presented the highest cumulative intensity of upwelling signals and the CMC data represents the lowest cumulative intensity of upwelling signals detected.

Table 2.10: Nested ANOVA evaluating the variation in upwelling cumulative intensity as detected in four gridded SST products (OISST, CMC, G1SST, and MUR) at several distances away from the shore and sites within the Benguela Current region of South Africa. Only the main effect due to 'product' is indicated. Comparisons are graphically captured in **Figure 2.10**.

	d.f.	M.S.	*F*-value	*P-value*
Product	3	4306	14.12	< 0.001
residuals	725	305		

Pearson correlation analyses revealed that the possibility of observing the same upwelling signal detected at 0 km from the coast, at 25 km and at 50 km from the coast respectively varied across the individual data products at each of the four sites (**Table 2.11**). Overall, it was found that upwelling signals occurred simultaneously at 0 km and at 25 km considerably more frequently than between 0 km and 50 km from the coastline. In addition, the likelihood of detecting upwelling signals at 50 km from the coastline were notably lower throughout all pairwise comparisons, apart from signals detected at Port Nolloth, using the CMC, MUR, and G1SST products.

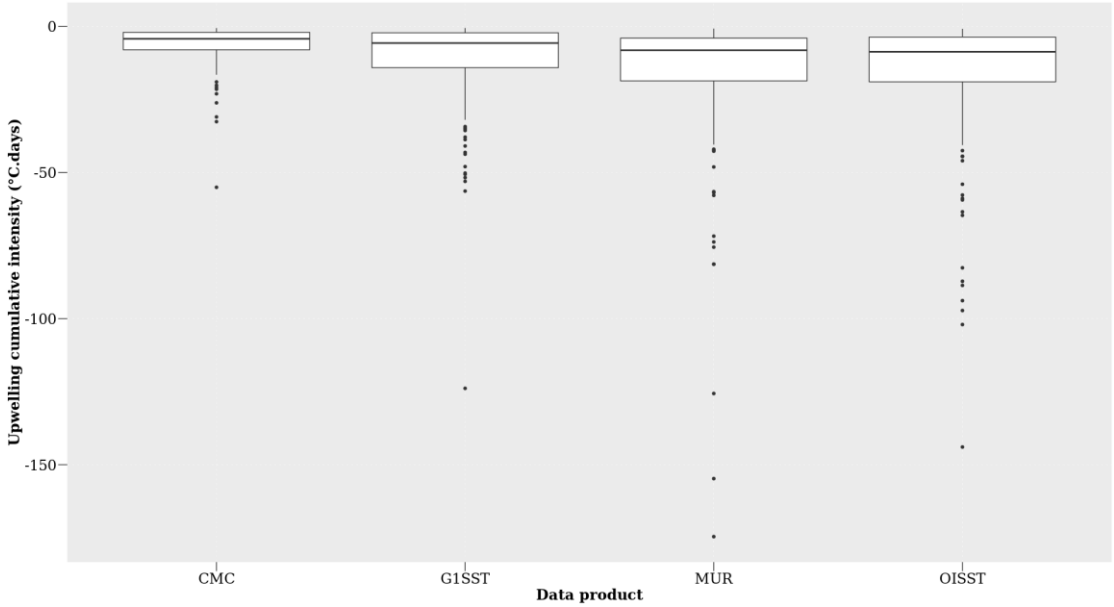

Figure 2.10: The cumulative intensity for each of the signals detected for the four satellite products at difference distances from the shore during summer months (December, January and February), over a four-year period.

Table 2.11: A Pearson correlation of the relationship between the number of signals detected at a distance of 0 km versus a distance of 25 km and between the number of signals at 0 km and 50 km.

Product	Site	0 km vs 25 km	0 km vs 50 km
OISST	Lamberts Bay	0.59	0.14
	Port Nolloth	0.76	0.38
	Saldanha Bay	0.65	0.42
	Sea Point	0.76	0.18
CMC	Lamberts Bay	0.12	0.05
	Port Nolloth	0.66	0.54
	Saldanha Bay	0.44	0.33
	Sea Point	0.69	-0.01
MUR	Lamberts Bay	0.60	0.29
	Port Nolloth	0.74	0.58
	Saldanha Bay	0.52	0.23
	Sea Point	0.63	0.42
G1SST	Lamberts Bay	0.73	0.32
	Port Nolloth	0.66	0.65
	Saldanha Bay	0.28	0.33
	Sea Point	0.57	0.30

The individual data products displayed different numbers of upwelling signals at distances of 0 km, 25 km, and 50 km from the coastline (**Figure 2.11**). There was no significant difference between the number of upwelling signals collected at the different sites (one-way ANOVA: $F = 2.27$, $d.f = 3$, SS = 2664, $p > 0.05$). However, there was a significant difference in the number of signals detected between products ($F = 53.53$, $d.f = 3$, SS = 13740, $p < 0.001$) and at different distances from the coastline ($F = 0.75$, $d.f = 2$, SS = 129, $p > 0.05$).

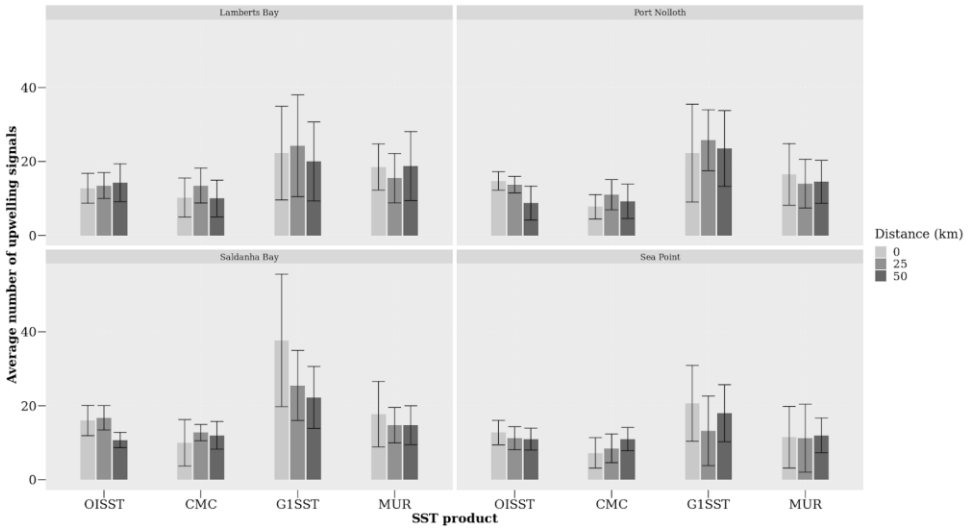

Figure 2.11: The average number of the signals detected at each site for the various satellite products from 2011 to 2014.

2.4. Discussion

2.4.1 Data products

The analyses in this paper showed that dissimilarities exist between products and sites when comparing the upwelling metrics. It was reported here that the highest resolution data, MUR and G1SST, which are available on a 0.01° grid, yielded the longest duration and cumulative intensity of upwelling signals compared to the coarser resolution data products. The MUR product, in particular, consistently yielded upwelling signals of the greatest intensity. Upwelling signals were most intense at the shore in all of the SST products. Analyses of the CMC, OISST and SACTN datasets revealed that recorded signals did not often exceed a duration of 10 days, whereas in MUR and G1SST the signals were detected for up to 14 days and even longer in some rare cases. Moreover, most of the signals detected in CMC, OISST and SACTN products only lasted for three days. This was similar for the higher resolution data products (G1SST and MUR) which also showed a high prevalence of signals lasting for just four days. In most cases, the number of signals detected at 0 km was higher than the number of signals detected at 50 km for the data products with the highest resolution. There was also a difference in mean intensity between products and distances from the site. The highest number of signals detected was recorded in the MUR and G1SST products.

Gridded datasets obtained from satellite imagery have provided an important understanding of offshore oceanographic processes and are reliable as they are usually spatially complete. However, coastal features such as upwelling cells are often smaller than the highest resolution of most SST products. In this study, estimates of upwelling duration, mean intensity and cumulative intensity (**Table 2.1)** may have been overestimated from data collected by the MUR and G1SST data products. These products are more likely to be susceptible to errors relating to limitations and data collection biases associated with satellite-derived sampling (Ricciardulli and Wentz, 2004; Liu et al, 2016), such as cases where there are large gaps within datasets that may have been caused by cloud cover or precipitation. These gaps are typically inferred from algorithms using past and forecasted data entries as well as data from nearby pixels which do not always reflect on real world patterns. For example, if upwelling signals were detected in an area that experienced extensive cloud cover over several weeks, the algorithm may suggest that upwelling continued throughout that period which may not have been the case. However, datasets constructed from multiple data sources, particularly from ships and buoys, are inherently more reliable in terms of reducing the frequency of falsely detecting signals as *in situ* help to prevent the SST algorithm from making interpolations away from reality (Smith and Reynolds, 2005; Kennedy et al., 2011). The overestimated data may be due to errors from different sources which are produced at each of the successive data processing level (Liu et al, 2016). For example, the Level 0 products (digitised detector output) to Level 4 products (bias corrected, geo-located, gridded, and gap-free SSTs). The SST accuracy refers to the retrieval error produced at Level 2 (derived SSTs at pixel bases), but Level 3 (binned, gridded and averaged Level 2 values) and Level 4 fields are extensively used in climate and modeling studies, mainly because of the desirable features of being “gridded and gap-free” (Liu et al, 2016). Another reason for this could be as a result of sampling error caused by incomplete coverage of satellite measurements. This incomplete coverage may be due to the presence of clouds causing gaps in the sampling of SST. Cloudy pixels rejected by SST cloud masks constitute up to 90% of the total sampled pixels (Liu et al, 2016) and because of gaps between successive swaths of some sensors which may cause sampling errors.

It is important to note that the data sources are intrinsically different in the ways in which they were obtained or recorded. Consequently, discrepancies between datasets are to be expected. For example, the SACTN *in situ* collected SST product will reflect the actual temperature of the water being measured but instrumental differences when using a thermometer or an electronic sensor will result in inconsistencies. This is particularly prevalent because satellite temperatures are collected remotely and sensors do not make contact with the water. Here, properties of infrared (IR) and microwave (MW) are related through complex algorithms to temperature (Minnett et al., 2002). Smit et al. (2013) showed that warm and cold biases exist along the southern and western coastal region of South Africa, and the juncture between upwelling and non-upwelling regions have a tendency to influence the variability and magnitude of the SST bias. When comparing SST products, a small bias is always likely to be present because of cloud cover and wind strength (Dufois et al., 2012). Overall, the different data products compared within this study yielded different results. While flagging techniques are supposed to occasionally flag good values (Kilpatrick et al., 2001), it was found that flagging may occasionally be too vigorous for EBUS (Dufois et al., 2012). For example, the flagging method used on an OISST reference test induces warm coastal bias in data from both the MUR and G1SST data during summer. It should be noted that this phenomenon can be explained by strong coastal SST gradients in these upwelling regions. Differences in observations of upwelling events between data products at different sites, and at various distances from the coastlines can be attributed to several facets relating to the measurement protocols of each product. For example, differences in algorithms, components, and resolutions are contributed to the variable observation. Pixel-based atmospheric corrections developed for oceanic applications often fail or are in appropriate at the coast, and flagging techniques used to de-cloud data are also know to reduce strong biases at a monthly scale with strong horizontal SST gradients especially in upwelling systems. Missing pixels at the land/sea edge or 'land bleed'—i.e. pixels not flagged as missing but which are influenced by land temperatures 'mixing' with the actual sea temperatures may also influence temperature data obtained. Contributing towards the magnitude of differences in upwelling signals detected between the different SST products are factors such as data resolution, proximity from the coastline, the presence or absence of upwelling cells or embayments.

2.4.2. Oceanography

Upwelling processes in the southern Benguela are highly influenced by bottom topography (Nelson and Hutchings, 1983). The continental shelf which forms the eastern boundary of the Cape Basin, defined roughly by the 200 m isobath, varies in width from the 10 km at prominent capes to 150 km near Port Nolloth. In the vicinity of the Cape Peninsula and Cape Columbine, the coastline is irregular and two canyons associated with these features cut into the shelf, in the direction parallel to the coast (Nelson and Hutchings, 1983). However, along the remaining portion of the west coast, canyons are rare. The Cape Basin is bounded in the north by the Walvis Ridge which runs from the coast at 18° S to the Atlantic Central Ridge in a south westerly direction (Nelson and Hutchings, 1983). In the south, it is bounded by the Agulhas Ridge, a less pronounced topographic feature running parallel to the Walvsis Ridge from the Agulhas Plateau (Nelson and Hutchings, 1983). The dynamic topography of the area is such that the Agulhas Current water is fed into the Benguela systems from south of the Agulhas Bank.

Upwellling in the BUS occurs in a number of distinct upwelling cells, which form at location of maximum wind stress curl, and where there is a change in the orientation of the coastline. Lutjeharms and Meeuwis (1987) distinguished eight different cells (Cunene, Namibia, Walvis Bay, Lüderitz, Namaqua, Columbine, Cape Peninsula and the Agulhas cell), Shannon and Nelson (1996) further included three more upwelling cells along the south coast. The Lüderitz cell was identified as the most intense cell. Given that this research study is restricted to the southern Benguela, discrete upwelling cells at Cape Columbine and the Cape Peninsula will be discussed (Nelson and Hutchings, 1983). The Cape Columbine and Cape Peninsula upwelling cells are identified as two distinct bands of cold water on the inner and mid-continental shelves at a depth of 0-100 m, where upwelling is generally more intense during summer (Nelson and Hutching, 1983). This cold water is apparent along the length of the on the inner (0-100 m) and mid-continental shelves (100-200 m) (Weeks et al., 2006). In the Cape Peninsula region, a change in SST is present at Port Nolloth notable owing to the combined effects of being at the point of the southern limit of the Cape Peninsula upwelling cell and the sudden broadening of the inner shelf immediately to the south of the Peninsula. At the Cape Peninsula latitude, cooler upwelled water (<14°C) is confined primarily to the narrow inner shelf and this is evident in our data as we observe the most intense upwelling signals closer to the shore. It is also evident that the high resolution G1SST and MUR data sampled in Lamberts Bay, Saldanha Bay and Sea Point show the highest number of upwelling signals detected at the narrow inner shelf with fewer signals collected at the mid latitude shelf. The findings made here further show that the coarser resolution (OISST) product fails pick up signals further offshore, as seen in Sea Point. Currie (1953) and Hart and Currie (1960) further explain that the BUS consists of a series of anticyclonic eddies of interlocking cool and warm water, which is in constant state of change. This allows for upwelling to not be uniform along the coast and found upwelling water to originate between 200 and 300 m deep. By understanding the topography, it is evident that, although upwelling is not visible at the surface, subsurface upwelling is possible (Nelson and Hutching, 1983). This further suggests that in cases when the same signal was detected at the shoreline and 25 km from the coast, a corresponding signal would not be identified at a distance of 50 km and this may be explained by sub-surface upwelling.

While the SST data may be satisfactory for interpretation of regional phenomena; SST suffers from several drawbacks when applied within the coastal region. Here the interaction of hydrodynamic and atmospheric forces creates a complex system which is influenced by larger variability at smaller spatial scales than further offshore (Dufois et al., 2012). Hydrodynamic regimes such as stratified water columns may break down at the coast in very shallow waters, and seawater temperatures measured there may not directly relate to SSTs measured further from the coast at the ocean's surface (Broitman et al., 2008). These inshore hydrodynamics may be described by a) the injection of turbulence through breaking waves, thus increasing the breakdown of the mixed layer; b) convective mixing due to the cooling through the process of evaporation, which occurs during winter months under cool dry air; c) tidal mixing which minimises the vertical thermal gradient; and d) mixing through velocity often caused by wind driven currents. Together, these processes homogenise the first few meters of the water column and therefore minimise the difference between the surface temperature and deeper bulk temperature (Minnett et al., 2004). In hydrodynamically active zones, such as the BUS, the absence of shallow stratification would cause a portion of cooler water than the bulk surface waters of the ocean to which satellite SSTs have been referenced. Thermal heating of coastal waters may also be exaggerated due to the proximity to the coast (Dufois et al., 2012). This type of heating is commonly seen in embayments, which reduce water exchange and limit wave activity and ultimately affect the deepening of the thermocline. These processes are highly variable on a spatial and temporal scale depending on the coastal bathymetry and wind regime.

2.4.3 Conclusion

Despite the influence of many oceanographic factors affecting the detection of upwelling signals, SST generally shows a high degree of correspondence with measurements obtained by buoys and other sources of *in situ* seawater temperature measurements (Donlon et al., 2002; Smit et al., 2013). However, although SST products developed offshore and within the oceanic regions are being applied to the coastal regions, reports exist to inform users to exercise caution when using SST datasets in these coastal regions (Tittensor et al., 2010). It should also be noted that the patterns visible within this study region may result because of different scales in signals causing only higher resolutions to be able to detect them. Upwelling signals are small signals (cold pulses of water that may last for a few hours or days), which may have contributed to the higher resolution (MUR and G1SST) products detecting more signals lasting for a longer period when compared to the coarser resolution products (e.g. OISST). Finally, the MUR SST showed the most promise in terms of a reliable source for detecting and quantifying upwelling metrics as it was able to accurately detect the same signals visible at 0 km and 50 km from the coastline. However, in a case where long term (> 30 years) trends of upwelling signals are being studied, the OISST dataset would be more suitable as this time series extends for more than three decades.

Data products of the highest resolution yield upwelling signals more abundantly and intensely closer to the shore in the inner continental shelf region as expected given the topographical differences along the coastline. Hence, we conclude that the higher resolution data are more accurate at detecting these fine scale cold pulses. This research not only provides us with a better method of detecting upwelling signals, which is useful to observe trends in upwelling signals overtime, but also emphasizes the importance of selecting the correct data product in concert with knowledge about the nature of the physical phenomena being studied. Detecting and monitoring upwelling is a useful tool for ecosystem management and better characterisation of oceanographic processes. While this SST approach to upwelling shows promise, the limitations and biases within SST data collection methods as well as other factors of near shore versus offshore, oceanographic phenomena, and spatial resolution are all important considerations that must be taken into account.

CHAPTER 3

VARIATION OF UPWELLING SIGNALS DETECTED IN EBUS

Abstract

Global increases in temperature are severely altering land-sea temperature gradients. Bakun (1990) hypothesised that changes within these gradients will directly affect atmospheric pressure cells associated with the development of winds, and will consequently impact upwelling patterns within ecologically important Eastern Boundary Upwelling Systems (EBUS), which often act as 'buffers' that protect marine communities from the effects of ocean warming. In this study I used NOAA Optimally Interpolated sea surface temperature (SST) and ERA 5 reanalysis wind products to calculate an upwelling index which was used to detect, identify and quantify upwelling signals that have occurred throughout these EBUS over time last 37 years during summer months. Overall SST increased at three of the four EBUS currents, but there was a decrease in the number of signals detected and no significant increase in the intensity of these signals. The Humboldt current system in particular showed opposite trends with a decrease in SST and increase in the number of upwelling signals detected. Overall, these findings do not agree with the Bakun hypothesis.

Keywords: Climate change, Upwelling, Seawater temperature, coastal regions, Code: R

3.1. Introduction

Coastal upwelling is a major oceanographic process driven by prominent currents within Eastern Boundary Upwelling Systems (EBUS) (Bakun and Nelson, 1991; Messié et al., 2009; Gruber et al., 2011; Pegliasco et al., 2015; Brady et al., 2019). EBUS include the California (CCS), Humboldt (HCS), Canary (CnCS) and Benguela (BCS) current systems (**Figure 1**), with each of these significantly impacting their associated coastal ecosystems. These systems are characterised as vast regions of coastal ocean occurring along the western shores of continents bordering the Pacific and Atlantic Oceans (Bakun, 1990; Pauly and Christensen, 1995; Bakun et al., 2010; Bakun et al., 2015). EBUS span a wide range of latitudes and are therefore spatially heterogeneous environments. The CCS experiences significant natural variability from sources such as El Niño-Southern Oscillation (ENSO) and the Pacific Decadal Oscillation (PDO) with important ecosystem consequences. The HCS environmental and biological diversity are also heavily influenced by ENSO. The CnCS is heavily influenced by the North Atlantic Oscillation (NAO). The BCS is unique as it experiences interannual variability in the physical and biological conditions related to Benguela Niños and the Pacific ENSO, and in the south, the BCS is largely influenced by the variability in the Agulhas Current (García-Reyes et al., 2015).

EBUS systems are a common source for oceanographic and biological research because the complex interplay of biotic and abiotic processes within EBUS areas results in them being highly productive, diverse, and abundant in marine life. EBUS regions provide up to 20% of the world's fishery output despite only covering <1% of global ocean area (refs.). The biological productivity in EBUS is mainly as a result of warm-season upwelling (Borges et al., 2003; Carr and Kearns, 2003; Chavez and Messié, 2009; Rossi et al., 2009; García-Reyes et al., 2013) which results from large-scale atmospheric pressure systems that favour along-shore, equatorial winds, in combination with the Coriolis effect that advects surface water offshore (Huyer, 1983; Seager et al., 2003; García-Reyes et al., 2015). These regions provide both lucrative economic as well as significant recreational services to 10s of millions of people living along these coastlines and indirectly to the rest of the world. However, recent studies have shown ecological changes in the EBUS ecosystem structure (Fréon et al., 2009; Syndman, et al., 2014; Wang et al., 2015), hence monitoring these systems is becoming increasingly important. EBUS form part of wind-driven ocean circulation, and their existence is entirely dependent on wind direction and strength (Capet et al., 2004). Recognising that the cross-shore atmospheric pressure gradients lead to alongshore, equatorward winds that drive coastal upwelling, Bakun (1990) hypothesised an increase in upwelling favourable winds over time due to intensification of the continental oceanic pressure gradient as a result of climate change (Bakun, 1990; Sydeman et al 2014; Garcia-Reyes et al., 2015). Understanding, therefore, how these winds will change is of high importance for anticipating how upwelling might respond. For example, weaker upwelling may limit nutrient enrichment and potentially impact primary production (Chhak and Di Lorenzo, 2007; García-Reyes et al., 2015). In contrast, stronger upwelling may increase nutrient input and therefore offshore transport (Bakun et al., 2010, 2015). Other impacts include changes in turbulence as a result of increased wind intensity (Cury and Roy, 1989) and changes in chemical mechanisms like ocean acidification and deoxygenation which may ultimately affect productivity (Gruber, 2011). Conservation of fisheries and resources within EBUS could be improved by understanding how nutrient enrichment and productivity are related to upwelling processes, and how likely they are to change in future climate change scenarios to fisheries yields.

Several recent studies have focused on assessing trends in upwelling favourable winds, with conflicting results being reported (refs. for intensifications; refs. against intensification). The failure to reach consensus revolves largely around the amplitude of unidirectional wind trends relative to amplitudes of seasonal, interannual, and decadal wind variability and the short duration of time series available relative to decadal variability Some researchers question whether the impacts of differential heating on the pressure gradient force drives intensification of coastal upwelling. Rather, a complementary hypothesis proposes that evidence of an intensifying pressure gradient force is limited to poleward migration of the Hadley Cell (Rykaczewski et al., 2015; Brady et al, 2017; Grise et al., 2019; Grise and Davis, 2020). Further complications preventing the agreement on findings in EBUS largely rely on (a) disparate data sets being examined, (b) inconsistencies in data treatment, including analyses of warm seasons versus annual means, (c) quality and density of the data, and (d) changes in measurement techniques An increase (decrease) in upwelling favourable winds can also amplify (reduce) the effect of coastal warming. Therefore, changes in upwelling favourable winds are likely to play an important role in upwelling-related ecosystem processes. Many of the significant upwelling modifications in EBUS, particularly in the Pacific Ocean, have been attributed to large scale atmospheric processes (Jacox et al., 2015). ENSO is the leading cause of variability in the HCS and CCS (Minobe et al., 1999). Other factors such as the Pacific Decadal Oscillation (PDO), and the North Pacific Gyre Oscillation (NPGO) are linked to the variability in the CCS (Chhak and Di Lorenzo, 2007; DiLorenzo et al., 2008). The BCS, however, is highly influenced by small scale variability and Benguela Niño (Chavex et al., 2009). No study, as yet, report shared variability and a consistent response across all EBUS.

In this context, the atmospheric and oceanic mechanics responsible for coastal upwelling are interdependent, and changes in one variable, such as wind speed can have an effect on other variables such as upwelling intensity. The focus of this study is to identify whether or not changes in upwelling-related atmospheric variables exist in these systems. The

timing and intensity of coastal upwelling are known to have a critical role in the phenology of key marine ecosystem process such as the recruitment of rocky intertidal organisms (Barth et al., 2007; McGregor et al., 2007). Changes in upwelling characteristics have been shown to cause substantial disturbances in ecosystems at multiple trophic levels. We therefore aim to detect if coupled changes occur in the (a) SST patterns, (b) intensity, duration and frequency of wind blowing in a south easterly direction, and (c) the frequency, mean and cumulative intensity of upwelling signals during summer months over a period of 37 years (**Table 3.1)**. Understanding changes within these systems could allow for predictive management and conservation of fisheries and marine resources.

Table 3.1: The description for the metrics of upwelling signals

Name (unit)	Definition
Duration (days)	Consecutive period of time that temperature exceed the threshold
Count (no. events per year)	Number of upwelling signals per year
Mean intensity (°C)	Mean temperature anomaly during the upwelling signal
Cumulative intensity (°C.days)	Sum of the daily intensity anomalies over the duration of the event

3.2. Methods

3.2.1. Data

To evaluate if there are changes in frequency, mean intensity and cumulative intensity of upwelling signals (**Table 3.1**), this study made use of the gridded data of the global 0.25° National Oceanic and Atmospheric Administration (NOAA) daily Optimally-Interpolated Sea Surface Temperature (dOISST, v.2) (Reynolds et al., 2007; Banzon et al., 2016). This product is constructed by combining different data collected from satellites, ships and buoys (Reynolds et al., 2007; Banzon et al., 2016). The OISST data product has been collected for more than four decades, hence providing us with a long (> 30 years) time series as defined by Hobday et al. (2016) from which upwelling trends and their rate of change can be calculated. Data products with a higher resolution often do not have a time series length of greater than 30 years. In order to detect variation in upwelling signals among the four EBUS (**Figure 3.1**) (Bakun, 1990; Bakun et al., 2015), wind speed and direction were also deemed as important variables, along with SST. Wind speed and direction variables were downloaded from the ERA5 climate reanalysis produced by ECMWF, providing daily data on regular latitude-longitude grids at 0.25° × 0.25° resolution.

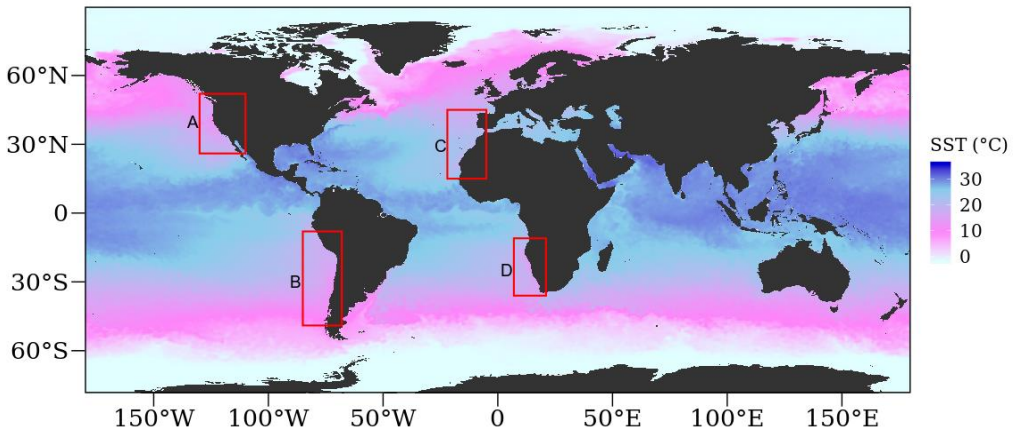

Figure 3.1: OISST throughout the global ocean. The red coloured rectangles delimit EBUS: A: California (CCS), B: Humboldt (HCS), C: Canary (CnCS) and D: Benguela (BCS) current systems.

3.2.2. Upwelling identification

In order to identify whether changes exist in the frequency and intensity of upwelling signals across EBUS it is important to first identify when upwelling occurs. In order to do this, a set of upwelling threshold values needed to be established. The method of determining upwelling signals considers both SST and wind variables which narrows these signals down to a more definite scale. Wind data were used in order to calculate the upwelling index using the formula presented in Fielding and Davis (1989):

$$upwelling\ index = \mu(\cos\theta - 160)$$

The index relies heavily on wind speed and direction in order to identify the presence of upwelling. An upwelling index < 0 represents downwelling whilst an upwelling index > 0 represents upwelling (Fielding and Davis, 1989). An upwelling index > 0 suggests a dropping SST as indicative of active upwelling. This drop in SST coincides with the seasonal SST variation at the 25th percentile threshold. Thus, the combination of SST and upwelling index value was used to identify upwelling. It was then necessary to identify the number of consecutive days that must be exceeded for an upwelling signal to be identified as a discrete event. Here it must be noted that upwelling is known to vary on a seasonal basis and may also occur hourly (sub-daily). Therefore, the minimum duration for the classification of an upwelling signal was set as one day. The rationale behind this is that the OISST dataset is available at a daily resolution. With the upwelling index, temperature and duration thresholds established, the detect_event() function from the **heatwaveR** package (Schlegel and Smit, 2018) was used to calculate metrics for the upwelling signals. By using this method of identifying signals, we were able to obtain upwelling metrics such as the frequency of occurrence ('frequency'), 'mean intensity,' and 'cumulative intensity.' Here, we defined the mean intensity of temperature (°C) represented the highest temperature anomaly value throughout the duration of the signal. Cumulative intensity (°C.days) was defined as the sum of daily intensity anomalies across the duration of each event. Because upwelling signals were calculated relative to seasonal climatologies of percentile exceedances, rather than an absolute definition such as temperatures below a fixed temperature threshold, these signals could occur any time of the year; however, upwelling was shown to be more dominant during summer months, as expected.

With upwelling being influenced by wind patterns, Bakun (1990) predicted that changes in wind patterns would influence the intensity of upwelling signals. As a first step, I observed trends in SST; this was done to simply understand how SST data within these cold-water regions are changing over time. I selected all coastal SST pixels along the latitudinal bands shown for each EBUS in **Figure 3.1**, as the coastal region is the most favoured to either live permanently, for leisure, recreational activities, or tourism. Given that the OISST time series length is greater than 30 years it is possible to discern the long-term trends within the data. Using a linear regression analyses, I observed if changes exist in the number of times wind blew in south easterly (SE) direction, the duration of SE winds, and intensity of wind blowing in a SE direction with an emphasis on austral (DJF) and boreal (JJA) summer months. The month variable was selected to observe which month expressed the most intense signal. To establish whether differences existed between current and upwelling metrics overtime, I assessed the upwelling metrics as a function *year* or *month*. Thereafter, using regression analysis, I compared the average numbers of upwelling signals detected in each of the currents.

3.3. Results

Table 3.2: Linear regressions displaying yearly differences in south-easterly (SE) directed winds and upwelling metrics over a period of 37 years.

EBUS	BCS	HCS	CCS	CnCS
SST	+ve (R^2 = 0.09, slope = 0.01, p < 0.001)	-ve (R^2 = 0.08, slope = -0.007, p < 0.001)	+ve (R^2 = 0.04, slope = 0.01, p < 0.01)	+ve (R^2 = 0.03, slope = 0.009, p < 0.01)
No. of SE directed winds	0 (R^2 = 0.02, slope = -0.004, p > 0.05)	-ve (R^2 = 0.003, slope = -0.002, p > 0.05)	+ve (R^2 = 0.14, slope = 0.008, p < 0.001)	0 (R^2 = 0.007, slope = 0.001, p > 0.05)
SE directed wind duration	0 (R^2 = 0.02, slope = -0.005, p > 0.05)	0 (R^2 = 0.005, slope = -0.006, p > 0.05)	+ve (R^2 = 0.06, slope = 0.003, p < 0.001)	0 (R^2 = 0.004, slope = -0.001, p > 0.05)
SE directed wind intensity	0 (R^2 = 0.002, slope = 0.004, p > 0.05)	0 (R^2 = < 0.001, slope = -0.002, p > 0.05)	0 (R^2 = 0.005, slope = 0.008, p > 0.05)	0 (R^2 = 0.01, slope = 0.001, p > 0.05)
No. of upwelling signals	0 (R^2 = 0.02, slope = -0.002, p > 0.05)	+ve (R^2 = 0.06, slope = 0.005, p < 0.005)	-ve (R^2 = 0.09, slope = -0.006, p < 0.005)	-ve (R^2 = 0.13, slope = -0.007, p < 0.005)
Mean intensity	-ve (R^2 = 0.04, slope = -0.001, p < 0.05)	-ve (R^2 = 0.19, slope = -0.003, p < 0.001)	-ve (R^2 = 0.09 slope = -0.001, p < 0.001)	+ve (R^2 = 0.09, slope = 0.001, p < 0.005)
Cumulative intensity	0 (R^2 = 0.09 slope = -0.001, p < 0.005)	-ve (R^2 = 0.16, slope = -0.04, p < 0.001)	-ve (R^2 = 0.007, slope = -0.008, p > 0.05)	+ve (R^2 = 0.08, slope = 0.02, p < 0.001)

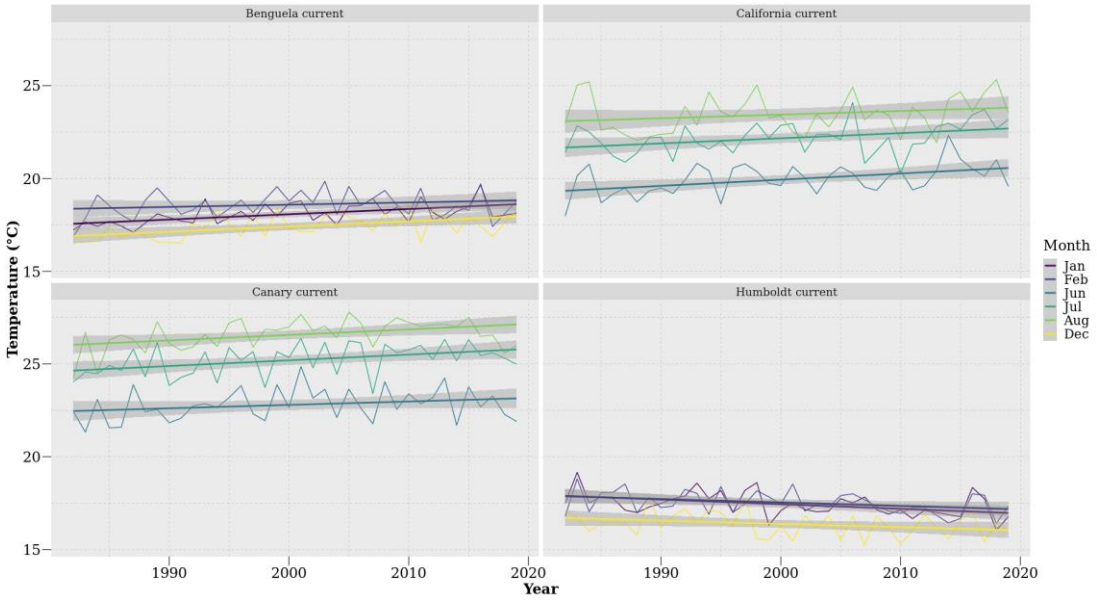

Figure 3.2: SST trends during austral (DJF) and boreal (JJA) summer months over 37 year.

My investigations of upwelling trends within individual time series data for each of the four EBUS currents revealed that changes in SST patterns have occurred at each site over the past 37 years (**Figure 3.2**). The BCS displayed a slow positive increase in SST of approximately 0.17 ± 0.02 °C.dec^{-1}, with increases being particularly prominent during January of each year. Similarly, the CCS also showed an increase in SST with a positive trend of 0.20 ± 0.02 °C/decade, with its steepest increases occurring during June. The CnCS continually showed warming trends of 0.20 ± 0.01 °C.dec^{-1}, with August representing the month with the steepest increase of 0.20 °C.dec^{-1}. Overall, the SST of the BCS and CnCS currents both increased by approximately 0.21 °C over a period of 37 years. Results obtained from a regression analysis suggested an increase in SST over time with a positive trend in the BCS (R^2 = 0.09, slope = 0.01 °C.yr^{-1}, p < 0.001), HCS (R^2 = 0.08, slope = -0.007 °C.yr^{-1}, p < 0.001), CnCS (R^2 = 0.03, slope = 0.009 °C.yr^{-1}, p < 0.01) and CCS (R^2 = 0.04, slope = 0.01 °C.yr^{-1}, p < 0.01). Conversely, the HCS displayed a negative trend that was strongest during January (R^2 = 0.18, slope = -0.02 °C.yr^{-1}, p < 0.005) and February (R^2 = 0.11, slope = -0.02 °C.yr^{-1}, p < 0.05) of each year respectively. A prominent positive trend was present in the CCS during June (R^2 = 0.19, slope = 0.03 °C.yr^{-1}, p < 0.005) and July (R^2 = 0.13, slope = 0.01 °C.yr^{-1}, p < 0.01). A similar trend was present in the CnCS during July (R^2 = 0.17, slope = 0.03 °C.yr^{-1}, p < 0.01) and August (R^2 = 0.17, slope = 0.03 °C.yr^{-1}, p < 0.01).

The trend in count of periods of south-easterly directed winds was not uniform among the four EBUS (**Figure 3.3**). A linear regression analysis showed no significant trends in the number of wind events detected in the BCS (R^2 = 0.02, slope = -0.004 count.yr^{-1}, p > 0.05), CnCS (R^2 = 0.007, slope = 0.001 count.yr^{-1}, p > 0.05) and HCS (R^2 = 0.003, slope = -0.002 count.yr^{-1}, p > 0.05). However, a positive trend in the count of wind events was found in the CCS (R^2 = 0.14, slope = 0.008 count.yr^{-1}, p < 0.001) (**Table 3.2)**. This trend is particularly prominent during July (R^2 = 0.22, slope = 0.03 count.yr^{-1}, p < 0.005) and August (R^2 = 0.23, slope = 0.02 count.yr^{-1}, p < 0.001).

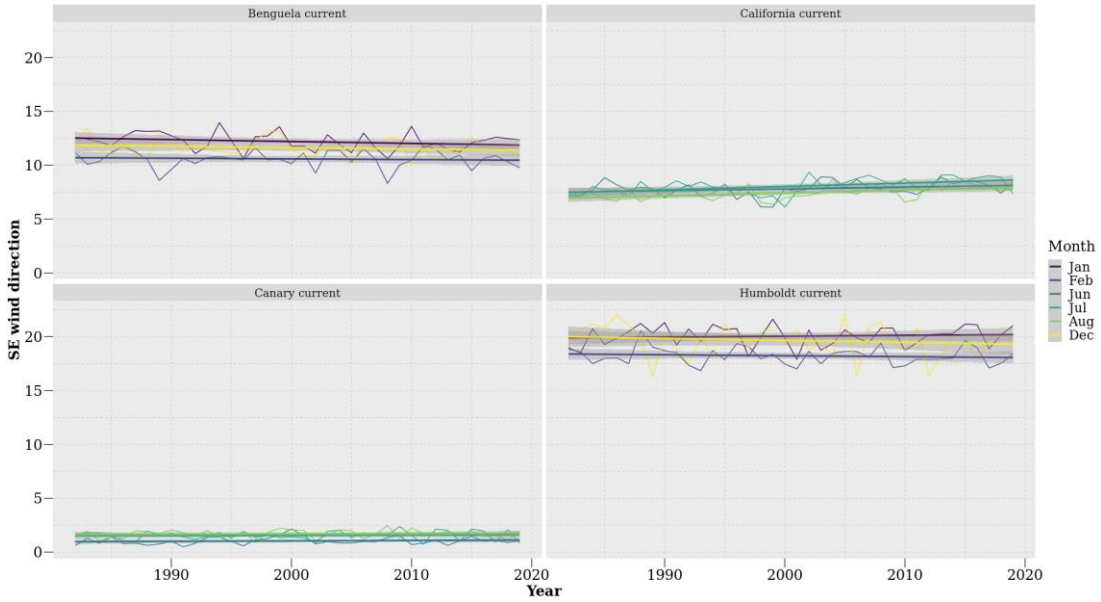

Figure 3.3: Counts of south-easterly directed winds during austral (DJF) and boreal (JJA) summer months over a period of 37 year.

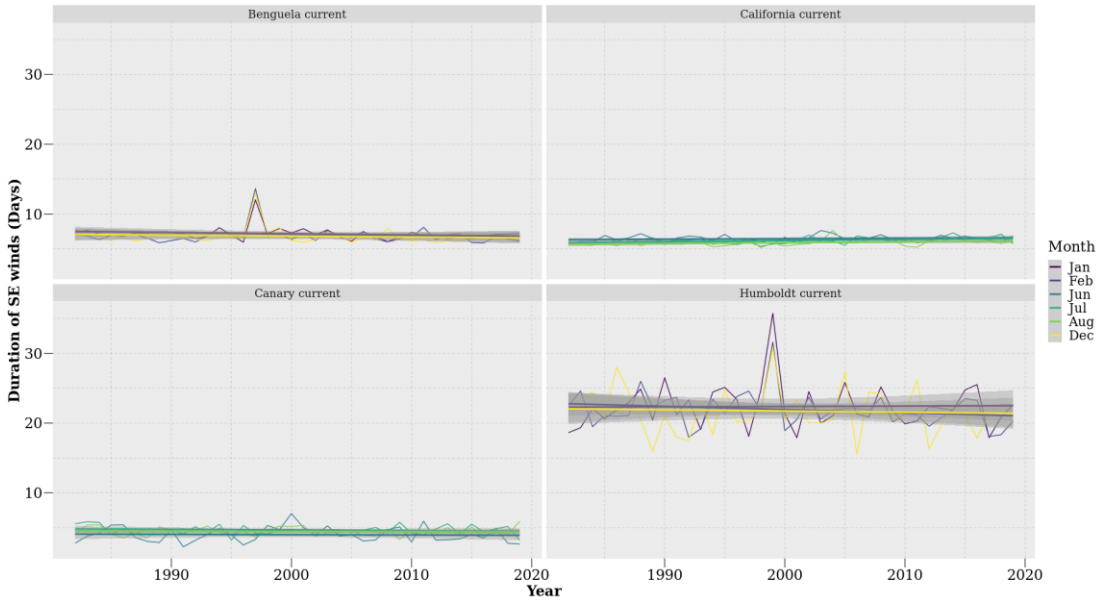

Figure 3.4: Duration of south-easterly directed winds during austral (DJF) and boreal (JJA) summer months over a period of 37 year.

The typical duration of south-easterly directed winds in the BCS, CCS and CnCS appeared to be short, lasting for less than 10 days. Conversely, winds in the HCS often exceeded 20 days (**Figure 3.4**). Results obtained from a linear regression suggested no change in trend in the duration of south-easterly directed winds in the $R^2 = 0.02$, slope = -0.005 days.yr^{-1}, $p > 0.05$), HCS ($R^2 = 0.005$, slope = -0.006 days.yr^{-1}, $p > 0.05$) and CnCS ($R^2 = 0.004$, slope = -0.001 days.yr^{-1}, $p > 0.05$). The CCS ($R^2 = 0.06$, slope = 0.003 days.yr^{-1}, $p < 0.001$), however, showed a slight increase in the duration of south-easterly directed winds with a positive trend particularly prominent during July ($R^2 = 0.16$, slope = 0.02 days.yr^{-1}, $p < 0.01$; **Table 3.2)**.

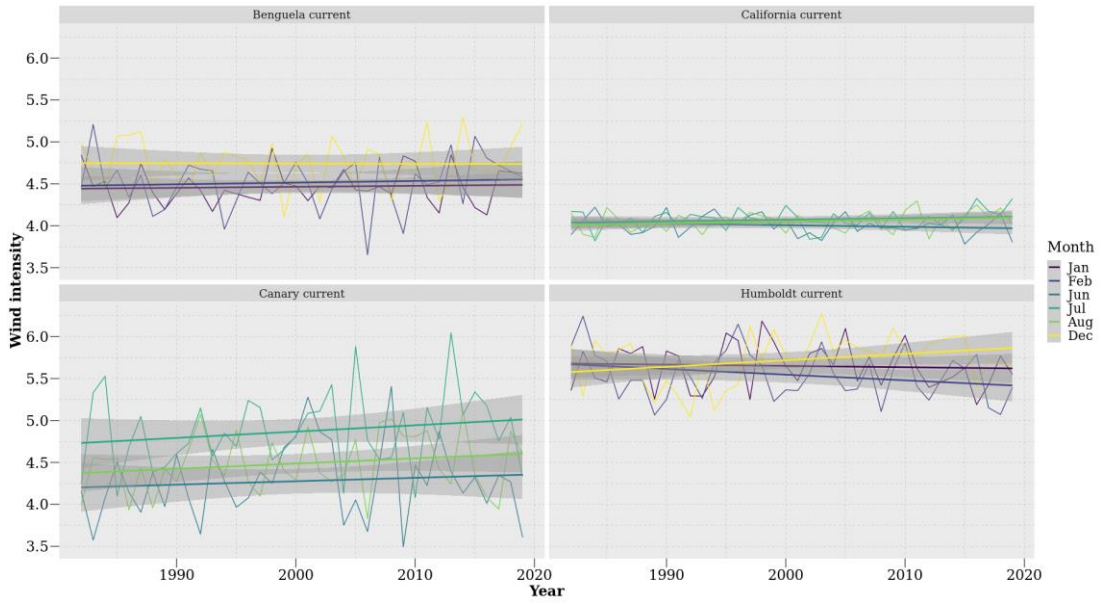

Figure 3 5: The intensity of south-easterly directed winds during austral (DJF) and boreal (JJA) summer months over a period of 37 year.

South-easterly winds were most intense in the HCS (**Figure 3.5**), where they often exceeded speeds of 5.5 $m.s^{-1}$. Winds were least intense in the CCS with speeds of approximately 4 $m.s^{-1}$ being commonplace. There were no changes in trends of wind intensity over time in the BCS (R^2 = 0.002, slope < 0.0004 $m.s^{-1}.yr^{-1}$, p > 0.05), HCS (R^2 = 0.001, slope < -0.001 $m.s^{-1}.yr^{-1}$, p > 0.05), CnCS (R^2 = 0.01, slope < 0.002 $m.s^{-1}.yr^{-1}$, p > 0.05) or CCS (R^2 = 0.005, slope < 0.005 $m.s^{-1}.yr^{-1}$, p > 0.05) (**Table 3.2)**.

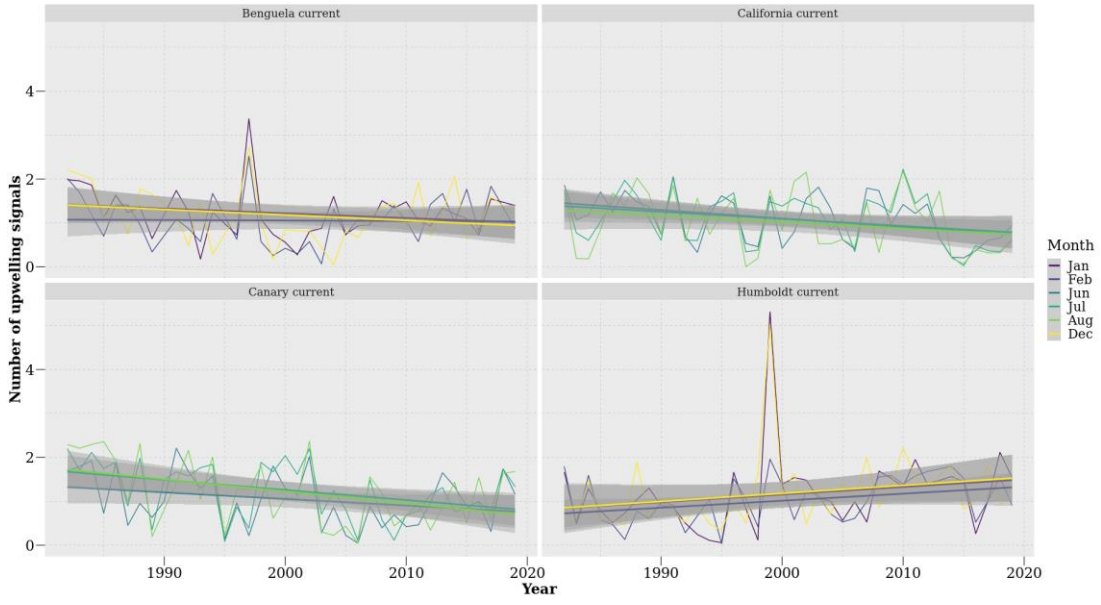

Figure 3.6: Number of upwelling signals detected during austral (DJF) and boreal (JJA) summer months over a period of 37 year.

I found that the number of upwelling signals detected decreased over time in the BCS, CCS and the CnCS, and slightly increased within the HCS current (**Figure 3.6**). This increase is particularly dominant during December (R^2 = 0.06, slope = 0.02 $count.yr^{-1}$, p < 0.005), supporting with decreasing SST temperature values. Results obtained from a regression analysis revealed no change in trend of the BCS (R^2 = 0.02, slope = -0.002 $count.yr^{-1}$, p > 0.05) a positive trend in the HCS (R^2 = 0.06, slope = 0.005 $count.yr^{-1}$, p < 0.005) which was strongest during Feb (R^2 = 0.12, slope = 0.02 $count.yr^{-1}$, p < 0.05). Negative trends in the number of upwelling signals occurred in the CCS (R^2 = 0.09, slope = -0.006 $count.yr^{-1}$, p < 0.005) and CnCS (R^2 = 0.13, slope = -0.007 $count.yr^{-1}$, p < 0.0001) (**Table 3.2**).

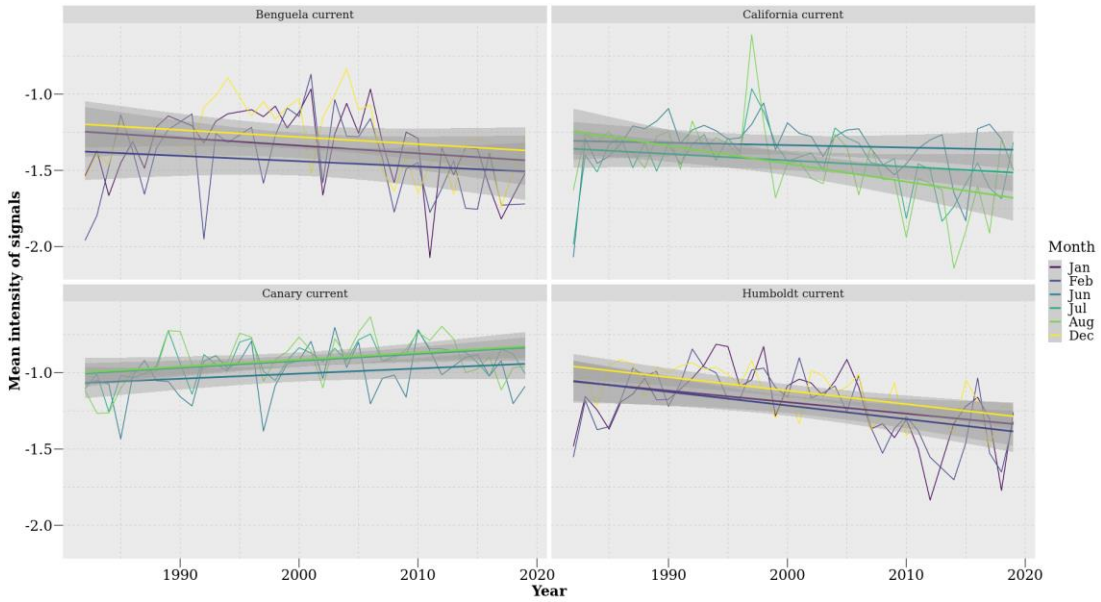

Figure 3.7: Mean intensity of upwelling signals detected during austral (DJF) and boreal (JJA) summer months over a period of 37 year.

The mean intensity of upwelling signals detected decreased over time in the BCS, CCS and the HCS, and slightly increased within the CnCS current (**Figure 3.7**). A regression analysis further suggested a negative trend which is associated with an increase mean intensity in the BCS (R^2 = 0.04, slope = -0.001 °C.yr^{-1}, p < 0.05), HCS (R^2 = 0.19, slope = - 0.003 °C.yr^{-1}, p < 0.001), CCS (R^2 = 0.09 slope = -0.001 °C.yr^{-1}, p < 0.001). The CnCS (R^2 = 0.09, slope = 0.001 °C.yr^{-1}, p < 0.005) however express a positive trend which is associated with a decrease in mean intensity (**Table 3.2**). Similarly, in the HCS a dominant negative trend persists during February (R^2 = 0.19, slope -0.009 °C.yr^{-1}, p < 0.005) and December (R^2 = 0.37, slope = -0.008 °C.yr^{-1}, p < 0.001) and during Aug in the CCS (R^2 = 0.25, slope = 0.01 °C.yr^{-1}, p < 0.001). In the CnCS, a positive trend was present during July (R^2 = 0.19, slope = 0.004 °C.yr^{-1}, p < 0.001) and August (R^2 = 0.11, slope = 0.004 °C.yr^{-1}, p < 0.001).

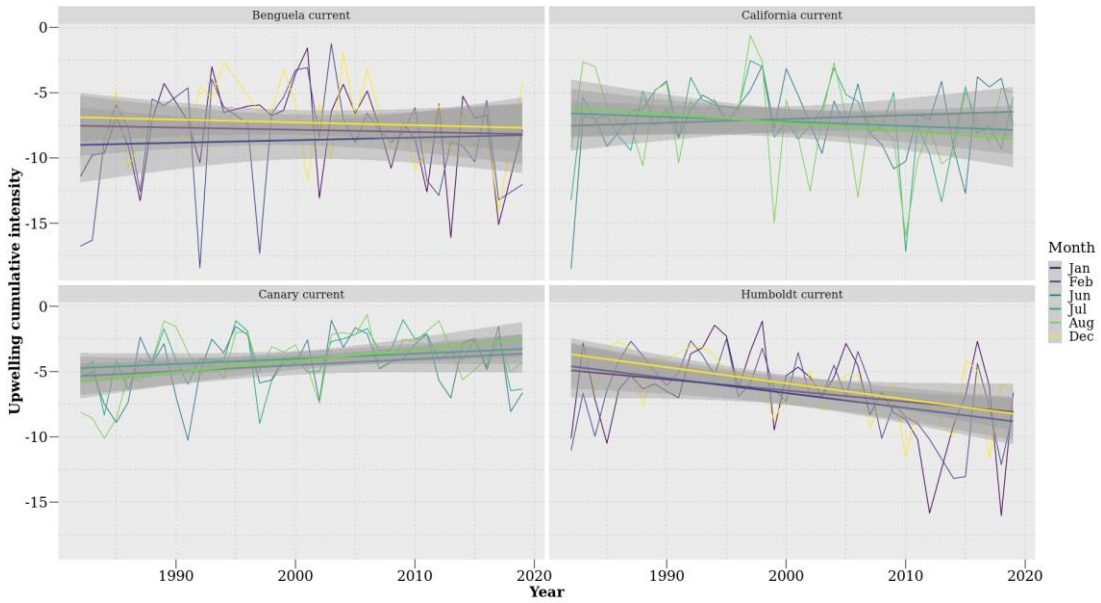

Figure 3.8: Cumulative intensity of upwelling signals detected during austral (DJF) and boreal (JJA) summer months over a period of 37 year.

Figure 3.8 shows a slight decrease in cumulative intensity in the CnCS. The HCS however showed a distinct increase in cumulative intensity over time. The results obtain from a regression analyses further suggest no change in trend occurs within the BCS (R^2 = 0.001, slope = -0.003 °C.days.yr^{-1}, p > 0.05). However, a negative trend was present in the HCS (R^2 = 0.16, slope = -0.04 °C.days.yr^{-1}, p < 0.001) and CCS (R^2 = 0.007, slope = -0.008 °C.days.yr^{-1}, p > 0.05) followed

by a slightly positive trend in the CnCS (R^2 = 0.08, slope = 0.02 °C.days.yr^{-1}, p < 0.001) (**Table 3.2**). The HCS showed a prominent negative monthly trend during Feb (R^2 = 0.19, slope = -0.11 °C.days.yr^{-1}, p < 0.005) and Dec (R^2 = 0.34, slope = -0.12 °C.days.yr^{-1}, p < 0.001). In the CnCS a positive trend persisted during Aug (R^2 = 0.17, slope = 0.09 °C.days.yr^{-1}, p > 0.05)

3.4. Discussion

Bakun (1990) proposed that an increase in greenhouse gases will result in considerable change in land-sea pressure gradients that will affect global wind patterns and ultimately result in an increase in the intensity of upwelling signals across the world's oceans. Here, I tested this hypothesis by analysing upwelling trends at four prominent upwelling regions, with an emphasis on austral (DJF) and boreal (JJA) summer months as this is when upwelling is most dominant. My results yielded weak evidence for increases in the intensity of upwelling signals across the southern and northern hemispheres of the world's coastal upwelling regions. Rather, the mean intensity of upwelling signals decreased in the BCS, HCS and CCS. However, the CnCS showed a slight increase in the mean intensity of upwelling signals over time. Given that upwelling signals did not intensify in all of the EBUS, I further investigated if SST and wind patterns have changed there over time. When observing the SST patterns within EBUS currents it was evident that the average temperature across all EBUS currents is continually increasing, except at the HCS. The same was not true of wind intensity, as I found no significant relationship between increased wind intensity and time at the different EBUS regions. Similarly, I found no difference in the duration and number of wind events blowing in a south easterly direction for the BCS, HCS, CnCS. However, there was a significant increase in the duration of wind events and in number of wind events blowing in a south easterly direction for the CCS. By combining wind and SST products I was able to observe trends in the number of upwelling signals detected. Our results suggested a decrease in the number of upwelling signals detected in three of the EBUS, except for the HCS, which showed an increase in the number of upwelling signals but no associated increase in wind duration/intensity detected over a period of 37 years. It was also particularly interesting to observe no increase in the mean intensity, cumulative intensity and number of upwelling signals detected of the CCS given this current was associated with an increase in the duration and number of south easterly winds. These findings do not agree with the hypothesis proposed by Bakun (1990) as the wind intensity did not intensify overtime and the resultant mean intensity of upwelling signals did not increase.

Given my findings here, it is evident that the effects of anthropogenic changes towards altering patterns of upwelling are more complex than proposed by Bakun (1990). It demonstrates the need to consider changes in both thermal and in-shore hydrodynamic (turbulence through breaking waves, tidal mixing and wind driven currents) processes when interpreting the full dynamical response (e.g. in conditions of changing wind magnitude and direction) of the coupled atmospheric-ocean system to climate warming. In this regard, our conclusion differs in respect to recent studies (e.g. Wang et al., 2015) that have examined the relationship between increasing summertime land-sea temperature differences and intensified upwelling in response to climate change. Rykaczewski et al. (2015) suggested that increased land-sea temperature differences are ubiquitous into projections of future conditions, but that summertime upwelling is limited to the polar extremes of upwelling zones. If true, this would indicate that increased land-sea temperature differences do not have a dominant influence on upwelling intensity. Additionally, changes in upwelling favourable winds are not always directly related to broad increases in land-sea temperature differences associated with climate change (Rykaczewski et al., 2015). Instead, the intensity of upwelling-favourable winds could be related to shifts in seasonal development and geographic positioning of the four major atmospheric high-pressure systems that are completely unrelated to anthropogenic influences. Research suggest that changes in sea level pressure (SLP) fields are expected in response to increased greenhouse gas concentration (Gillett et al., 2013; Griffies et al., 2014); these shifts will initiate changes in the magnitude, location and timing of upwelling favourable winds that are more consequential than increase land-sea temperature differences.

The results obtained in this study do not support the hypothesis that intensified upwelling will result from the increased land-sea difference associated with global warming. Additionally, given the short time series it is highly likely that a natural climatic variable impacted the trends discussed. For example, the occurrence of ENSO at the end of the time series could also have initiated an anomalously warm SST in EBUS and potentially affect the trends observed. Further investigation is required to fully explain the observed trends of upwelling within EBUS regions. Such investigations should ideally directly focus on the impact of inter-annual variability within individual EBUS currents. My results also lead to speculation about the potential connection between ENSO within EBUS (Peterson and Schwing, 2003; Blamey et al., 2012; Sydeman et al., 2013). ENSO represents a weakening of the Walker cell circulation (Wang, 2004). During normal Walker cell conditions there is consistent upwelling, and this upwelling contributes to cool SST (Bakun, 2010). Since the CnCS data show an increase in SST, it may also be concluded that there has been a weakening or reversal of the trade winds and a resultant El Niño is occurring (Vallis 1986; Saji et al., 1999). ENSO sends out atmospheric and oceanic Rossby waves that can have an effect on climate processes (Battisti, 1989; Holbrook et al., 2011). The effects ENSO has on its counterpart La Niña produces teleconnection that alter average climatic states (Diaz et al., 2001; Fogt

and Bromwich, 2006; Yeh et al., 2018). As a result, it can also be assumed that the weakening of HCS is potentially represented as a consequence of the effects by La Niña. During La Niña, the Walker cell circulation is enhanced (Sohn et al., 2013), meaning that pre-existing trade winds and SST strengthen. The low SSTs created by the presence of La Niña is accompanied by anticyclones. The anticyclones rotate counter-clockwise in the southern hemisphere and therefore its winds travel equatorward where they deflect surface water away from the shore, resulting in a net Ekman veering that encourages coastal upwelling and lowers SSTs. The HCS possessed the strongest winds when compared to the other EBUS. These winds consist of dry air creating climatic conditions that encourage evaporation. Evaporation requires heat, and this heat is supplied by the sea surface. Since evaporation takes heat away from the sea surface it has an overall cooling effect. For the CnCS, the enhanced evaporation caused by the strong offshore winds result in a cooling of the current system's SSTs. This upwelling system is typically characterised by generating a climate with low cloud coverage. Low cloud coverage allows for a high amount of solar radiation to be received at the ocean's surface.

There is low confidence regarding the effects of climate change on coastal temperatures and biogeochemistry in the EBUS. However, consideration is now given to shifts in the intensity and latitudinal location of upwelling and will be essential for identifying portions of the coast more at risk of ocean acidification, increased hypoxia, and eutrophication under conditions of future warming (Rykaczewski et al., 2015). This is primarily due to the complex global and local processes affecting these patterns, but also largely due to the resolution and data availability combined with the large degree of decadal variability in temperatures and biogeochemical properties. Most of the remotely sensed SST and wind products do not have sufficient resolution to accurately detect nuances within the upwelling process. Nevertheless, these data sources show promise in correcting bias by including higher-resolution products which consider land-and ocean-air interactions, cloud formation, and oceanic mesoscale processes. Furthermore, changes in local, alongshore winds are among one of several processes necessary to consider when exploring the sensitivity of upwelling in relation to climate change (Bakun et al., 2015). Waters supplied to upwelling systems, including nutrient concentrations, as well as the characteristics of the ocean carbonate system, and dissolved oxygen levels are sensitive to climate change (Rykaczewski et al., 2010) and have important ecological impacts (Lu et al., 2010).

In conclusion, my findings reject the hypothesis proposed by Bakun (1990). Wind events blowing in a south easterly direction did not increase or intensify over time, and importantly a negative trend exists in three of the four EBUS with the CnCS being the only current to display a slight increase in the mean and cumulative intensity of coastal upwelling signals. Therefore, there is an urgent need to carefully consider both geostrophic and ageostrophic processes affecting the boundary layer of the coastal ocean as these analyses may provide insight to the dynamics regulating changes in the upwelling. Additionally, changes in water-column stratification can alter upwelling efficacy (Roemmich and McGowan, 1995; Chhak and Di Lorenzo, 2007), and the offshore distribution of maximal upwelling (in addition to associated changes in wind-stress curl) can influence the rate and spatial location of upwelling (Rykaczewski et al., 2008; Jacox et al., 2014). Interactions among basin-scale processes and subsurface biogeochemistry that alter source-water properties of upwelled water masses, stratification, and mesoscale hydrographic features should be considered in concert with atmospheric forcing to develop a comprehensive understanding of the implications of climate change for the world's upwelling ecosystems. However, given the natural variability of EBUS, they are proven to be more resilient to climate change when compared to other ecosystems. The lack of expectations for EBUS ecosystems is of concern because these regions are biologically rich and as a result are highly relevant to society with regards to economics, conservation and biodiversity. Furthermore, I propose that the focus of this implementation be on nearshore ecosystems as these are more important to human livelihoods as well as being at greater risk when compared to other marine organisms.

CHAPTER 4

SYNTHESIS AND CONCLUSION

In the first study of this thesis, I used SACTN *in situ* collected data and satellite SST products to identify and compare upwelling signals at a variety of distances from the coastline. Here upwelling signals were used as a known signal in the data and allowed for a comparison between data products to quantify the efficacy of data products of differing resolutions. My findings here demonstrated the differences between SST products and their various resolutions. After demonstrating the capacity to identify upwelling signals using a novel method in the first study, the second study focussed on quantifying trends relating to upwelling signals within ecologically important EBUS currents over the past 37 years. Bakun (1990) proposed that climate change resulting from increased quantities of greenhouse gasses may fundamentally alter pressure gradients that will affect wind patterns and ultimately increase upwelling over prolonged periods. My results obtained from this study could not support Bakun's hypothesis. Importantly, the method used here differs from previous methods of identifying upwelling and currently represents the most effective means for identifying metrics of upwelling.

4.1. Contributions

I have presented a new method of detecting upwelling using SST and wind variable data. Prior studies on the matter, such as seen in Fielding and Davis (1989), often only consider wind measures to determine an upwelling index. My proposed method expands upon this by also including measures of SST, allowing for upwelling events as being defined when there were simultaneous drops in SST and a positive upwelling index. By using the `detect_event()` function in the **heatwaveR** package ((Schlegel and Smit, 2018) I was able to obtain distinct upwelling metrics (such as, mean intensity, cumulative intensity and duration) for each signal. This technique is useful as these quantifiable parameters can be calculated in an objective and consistent manner irrespective of geographical location. With these metrics, I was able to compare patterns in upwelling signals over time. The cumulative intensity metrics is perhaps the most important ecologically. As a product of duration and intensity, cumulative intensity can be used as an index to measure the threat of reduced upwelling on coastal systems. In Chapter 2, I used this method of determining upwelling, i.e. to compare differences in the counts, intensity and duration of upwelling signals at various distances from the coastline, and identified where upwelling was more dominant and intense. Using this method in Chapter 3, I identified signals which allowed me to observe patterns of upwelling within the world's four EBUS. Given the variable nature of my results, it became evident that further considerations on thermal and hydrodynamic processes relating to the upwelling process should be taken into account in future research that refines the process I developed above.

As seen in Chapter 2, the higher resolution data, the Group for High Resolution Sea Surface Temperature (G1SST) and Multi-scale Ultra-high Resolution (MUR) data products, detected signals lasting considerably longer and with higher cumulative intensity compared to the Optimally-Interpolated Sea Surface Temperature (OISST), Canadian Meteorological Center (CMC) and South African Coastal Temperature Network (SACTN) data products. The results also showed that upwelling varied at different distances from the coastline and that the higher resolution data would more likely detect upwelling further from the coastline compared to the lower resolution data. However, while higher resolution data produced overall superior detections, the limitations of the data products of broader resolutions did not severely alter the findings, although the effects due to data resolution were noticeable. The bathymetry within the Benguela Current region also plays an important role in affecting the detection of upwelling signals. Cooler upwelling waters are confined primarily to the narrow shelf allowing abundant and more intense upwelling to occur closer to the shore, and hence future research should primarily incorporate higher resolution datasets as these data are less likely to have incorrect readings and biases because they are obtained at a finer scale resulting in a more accurate product. Patterns obtained will then be more realistically reflected and minimise the likelihood of exaggerated detections.

By observing patterns of upwelling signals in EBUS for a period of 37 years, it is evident that the effects of anthropogenic changes towards altering upwelling intensity is more complex than proposed in the Bakun (1990) hypothesis. Here I show SST increased during summer months in all EBUS, except for the Humboldt current system (HCS). With this rise in SST, the number of upwelling signals appeared to have decreased over time, except for the HCS where an increase in the number of upwelling signals seemed apparent. I also showed that the intensity of upwelling signals did not increase over time in three of the four EBUS, with the CnCS being the exception. More importantly, wind patterns within the EBUS did not intensity over time as speculated by Bakun (1990). The mean intensity of upwelling showed a negative trend in three of the EBUS, with the CnCS being the only exception with showcasing a slight positive trend. It is also highly likely that a natural climatic variable (not accounted for in this study) impacted the trends observed in this study. For example, ENSO could have initiated anomalously warm SST when observing these trends.

4.2. Further research

The past decade has experienced development of several remotely-sensed SST products and blends of *in situ* and satellite data from diverse sources into a gap-free products useful to the marine science community. These products are under continuous revision, and each analysis enhances the quality of the data as algorithms are refined and the biases within the data are understood in more detail. Given that many factors that can influence how well SST products reflect climatological reality, several data products were used in this study to compensate for limitations and biases. However, because the data are collected at different resolutions, it is unsurprising that there are large discrepancies between data products. Satellite-derived data are obtained using instruments that are never in contact with the water, and hence the biophysical properties are sometimes related through inadequate algorithms to temperature. Further studies should aim at improving the proximity at which reliable data can be collected to the shore, which would enhance the detection of localised upwelling cells closer to the shoreline.

To better test the hypotheses proposed by Bakun (1990), future research should also seek to incorporate sea level pressure data and its trends overtime within EBUS. This should be done by observing summertime intensification between the temperature gradient and modifications to sea level pressure. As with many scientific fields, a greater knowledge of a subject often raises further questions which need answering. A range of further questions and data gaps were identified throughout my thesis. Understanding upwelling variability is important to assess marine ecosystem health, including that of factors such as ocean acidification and deoxygenation. Although the importance of upwelling is clear, reasons for the changes in upwelling metrics and the impact of anthropogenic climate change on these ecosystems are unclear. Changes in upwelling (count, metrics and duration) could affect marine ecosystems by influencing nutrient content into the euphotic zones if primary production is nutrient-limited. Changes in the phenology in upwelling winds may also affect trends within and across ecosystems as described here. Additionally, variation in the timing of upwelling strongly influences ecosystem productivity. Further research efforts should also focus on improvement of the methodology employed here to understand and include both atmospheric and oceanographic states during upwelling. The main goal of this thesis was not to predict events or signals but rather to use this novel method of determining upwelling signals and conduct an investigation into changes in trends in upwelling patterns over time. Ultimately the forecasting of upwelling signals should be used in conjunction with the adoption of subsequent future policies to better prepare for changes in these phenomena.

REFERENCES

Aguirre, C., Rojas, M., Garreaud, R.D., Rahn, D.A., 2019. Role of synoptic activity on projected changes in upwelling-favourable winds at the ocean's eastern boundaries. *npj Climate and Atmospheric Science*, *2*(1), pp.1-7.

Alves, J.M., Miranda, P.M., 2013. Variability of Iberian upwelling implied by ERA-40 and ERA-Interim reanalyses. *Tellus A: Dynamic Meteorology and Oceanography*, *65*(1), p.19245.

Arístegui, J., Barton, E.D., Álvarez-Salgado, X.A., Santos, A.M.P., Figueiras, F.G., Kifani, S., Hernández-León, S., Mason, E., Machú, E., Demarcq, H., 2009. Sub-regional ecosystem variability in the Canary Current upwelling. *Progress in Oceanography*, *83*(1-4), pp.33-48.

Arntz, W.E., Gallardo, V.A., Gutiérrez, D., Isla, E., Levin, L.A., Mendo, J., Neira, C., Rowe, G.T., Tarazona, J., Wolff, M., 2006. El Niño and similar perturbation effects on the benthos of the Humboldt, California, and Benguela Current upwelling ecosystems.

Auad, G., Miller, A. and Di Lorenzo, E., 2006. Long-term forecast of oceanic conditions off California and their biological implications. *Journal of Geophysical Research: Oceans*, *111*(C9).

Bakun, A., 1990. Global climate change and intensification of coastal ocean upwelling. *Science*, *247*(4939), pp.198-201.

Bakun, A., Nelson, C.S., 1991. The seasonal cycle of wind-stress curl in subtropical eastern boundary current regions. *Journal of Physical Oceanography*, *21*(12), pp.1815-1834.

Bakun, A., 1996. Patterns in the ocean: ocean processes and marine population dynamics, 323 pp. *University of California Sea Grant, San Diego & Centro de Investigaciones Biológicas del Noroeste, La Paz*.

Bakun, A., Weeks, S.J., 2004. Greenhouse gas buildup, sardines, submarine eruptions and the possibility of abrupt degradation of intense marine upwelling ecosystems. *Ecology Letters*, *7*(11), pp.1015-1023.

Bakun, A., Field, D.B., Redondo-Rodriguez, A.N.A., Weeks, S.J., 2010. Greenhouse gas, upwelling-favorable winds, and the future of coastal ocean upwelling ecosystems. *Global Change Biology*, *16*(4), pp.1213-1228.

Bakun, A., Black, B.A., Bograd, S.J., Garcia-Reyes, M., Miller, A.J., Rykaczewski, R.R. and Sydeman, W.J., 2015. Anticipated effects of climate change on coastal upwelling ecosystems. *Current Climate Change Reports*, *1*(2), pp.85-93.

Barange, M., Gibbons, M.J., Carola, M., 1991. Diet and feeding of Euphausia hanseni and Nematoscelis megalops (Euphausiacea) in the northern Benguela Current: ecological significance of vertical space partitioning. *Marine Ecology Progress Series*, pp.173-181.

Barth, J.A., Menge, B.A., Lubchenco, J., Chan, F., Bane, J.M., Kirincich, A.R., McManus, M.A., Nielsen, K.J., Pierce, S.D. and Washburn, L., 2007. Delayed upwelling alters nearshore coastal ocean ecosystems in the northern California current. *Proceedings of the National Academy of Sciences*, *104*(10), pp.3719-3724.

Barton, E.D., Field, D.B., Roy, C., 2013. Canary current upwelling: More or less?. *Progress in Oceanography*, *116*, pp.167-178.

Barton, C.A., McCormack, J.P., Eckermann, S.D., Hoppel, K.W., 2019. Optimization of Gravity Wave Source Parameters for Improved Seasonal Prediction of the Quasi-Biennial Oscillation. *Journal of the Atmospheric Sciences*, *76*(9), pp.2941-2962.

Battisti, D.S., 1989. On the role of off-equatorial oceanic Rossby waves during ENSO. *Journal of physical Oceanography*, *19*(4), pp.551-560.

Baumann, H., Doherty, O., 2013. Decadal changes in the world's coastal latitudinal temperature gradients. *PloS one*, *8*(6), p.e67596

Beaufort, L., de Garidel-Thoron, T., Mix, A.C., Pisias, N.G., 2001. ENSO-like forcing on oceanic primary production during the late Pleistocene. *Science*, *293*(5539), pp.2440-2444.

Belkin, I.M., 2009. Rapid warming of large marine ecosystems. *Progress in Oceanography*, *81*(1-4), pp.207-213.

Bjerknes, J., 1969. Atmospheric teleconnections from the equatorial Pacific. *Mon. Wea. Rev*, *97*(3), pp.163-172.

Blanco, J.L., Thomas, A.C., Carr, M.E., Strub, P.T., 2001. Seasonal climatology of hydrographic conditions in the upwelling region off northern Chile. *Journal of Geophysical Research: Oceans*, *106*(C6), pp.11451-11467.

Blanchette, M.L., Pearson, R.G., 2012. Macroinvertebrate assemblages in rivers of the Australian dry tropics are highly variable. *Freshwater Science*, *31*(3), pp.865-881.

Blamey, L.K., Howard, J.A., Agenbag, J., Jarre, A., 2012. Regime-shifts in the southern Benguela shelf and inshore region. *Progress in Oceanography*, *106*, pp.80-95.

Bograd, S.J., Schroeder, I., Sarkar, N., Qiu, X., Sydeman, W.J. and Schwing, F.B., 2009. Phenology of coastal upwelling in the California Current. *Geophysical Research Letters*, *36*(1).

Borges, M.F., Santos, A.M.P., Crato, N., Mendes, H., Mota, B., 2003. Sardine regime shifts off Portugal: a time series analysis of catches and wind conditions. *Scientia Marina*, *67*(S1), pp.235-244.

Boyd, A.J., Salat, J., Masó, M., 1987. The seasonal intrusion of relatively saline water on the shelf off northern and central Namibia. *South African Journal of Marine Science*, *5*(1), pp.107-120.

Boyer, D.C., Hampton, I., 2001. An overview of the living marine resources of Namibia. *African Journal of Marine Science*, *23*, pp.5-35.

Brasnett, B., 2008. The impact of satellite retrievals in a global sea-surface-temperature analysis. *Quarterly Journal of the Royal Meteorological Society*, *134*(636), pp.1745-1760.

Brady, R.X., Alexander, M.A., Lovenduski, N.S., Rykaczewski, R.R., 2017. Emergent anthropogenic trends in California Current upwelling. *Geophysical Research Letters*, *44*(10), pp.5044-5052.

Brady, R.X., Lovenduski, N.S., Alexander, M.A., Jacox, M. and Gruber, N., 2019. On the role of climate modes in modulating the air–sea CO2 fluxes in eastern boundary upwelling systems. *Biogeosciences*, *16*(2), pp.329-346.

Broitman, B.R., Mieszkowska, N., Helmuth, B. and Blanchette, C.A., 2008. Climate and recruitment of rocky shore intertidal invertebrates in the eastern North Atlantic. *Ecology*, *89*(sp11), pp.S81-S90.

Brown, O. B., Brown, J. W., Evans, R. H., 1985. Calibration of advanced very high resolution radiometer infrared observations. *Journal of Geophysical Research: Oceans*, *90*(C6), pp.11667-11677.

Bulgin, C.E., Embury, O., Merchant, C. J., 2016. Sampling uncertainty in gridded sea surface temperature products and Advanced Very High Resolution Radiometer (AVHRR) Global Area Coverage (GAC) data. *Remote Sensing of Environment*, *177*, pp.287-294.

Capet, X.J., Marchesiello, P., McWilliams, J.C., 2004. Upwelling response to coastal wind profiles. *Geophysical Research Letters*, *31*(13).

Cardone, V.J., Greenwood, J.G, Cane, M.A., 1990. "On trends in historical marine wind data." *Journal of Climate*, PP.113-127.

Carr, M.E., 2001. Estimation of potential productivity in Eastern Boundary Currents using remote sensing. *Deep Sea Research Part II: Topical Studies in Oceanography*, *49*(1-3), pp.59-80.

Carr, M.E., Kearns, E.J., 2003. Production regimes in four Eastern Boundary Current systems. *Deep Sea Research Part II: Topical Studies in Oceanography*, *50*(22-26), pp.3199-3221.

Casabella, N., Lorenzo, M.N., Taboada, J.J., 2014. Trends of the Galician upwelling in the context of climate change. *Journal of sea research*, *93*, pp.23-27.

Chao, Y., Li, Z., Farrara, J. D., Hung, P. (2009). Blending sea surface temperatures from multiple satellites and in situ observations for coastal oceans. *Journal of atmospheric and oceanic technology*, *26*(7), pp.1415-1426.

Chaigneau, A., Eldin, G., Dewitte, B., 2009. Eddy activity in the four major upwelling systems from satellite altimetry (1992–2007). *Progress in Oceanography*, *83*(1-4), pp.117-123.

Chavez, F.P., Messié, M., 2009. A comparison of eastern boundary upwelling ecosystems. *Progress in Oceanography*, *83*(1-4), pp.80-96.

Chhak, K., Di Lorenzo, E., 2007. Decadal variations in the California Current upwelling cells. *Geophysical Research Letters*, *34*(14).

Cury, P. and Roy, C., 1989. Optimal environmental window and pelagic fish recruitment success in upwelling areas. *Canadian Journal of Fisheries and Aquatic Sciences*, *46*(4), pp.670-680.

Cole, D., 1999. *Franz Boas: the early years, 1859-1906*. Douglas & McIntyre.

Cowtan, K., Rohde, R., Hausfather, Z., 2018. Evaluating biases in sea surface temperature records using coastal weather stations. *Quarterly Journal of the Royal Meteorological Society*, *144*(712), pp.670-681.

Cury, P. and Shannon, L., 2004. Regime shifts in upwelling ecosystems: observed changes and possible mechanisms in the northern and southern Benguela. *Progress in Oceanography*, *60*(2-4), pp.223-243.

Dewitte, B., Vazquez-Cuervo, J., Goubanova, K., Illig, S., Takahashi, K., Cambon, G., Purca, S., Correa, D., Gutiérrez, D., Sifeddine, A., Ortlieb, L., 2012. Change in El Nino flavours over 1958–2008: Implications for the long-term trend of the upwelling off Peru. *Deep Sea Research Part II: Topical Studies in Oceanography*, *77*, pp.143-156.

Diaz, H.F., Hoerling, M.P. and Eischeid, J.K., 2001. ENSO variability, teleconnections and climate change. *International Journal of Climatology: A Journal of the Royal Meteorological Society*, *21*(15), pp.1845-1862.

Diffenbaugh, N.S., Snyder, M.A., Sloan, L.C., 2004. Could CO2-induced land-cover feedbacks alter near-shore upwelling regimes?. *Proceedings of the National Academy of Sciences*, *101*(1), pp.27-32.

Di Lorenzo, E., Schneider, N., Cobb, K.M., Franks, P.J.S., Chhak, K., Miller, A.J., McWilliams, J.C., Bograd, S.J., Arango, H., Curchitser, E., Powell, T.M., 2008. North Pacific Gyre Oscillation links ocean climate and ecosystem change. *Geophysical Research Letters*, *35*(8).

Doney, S.C., Ruckelshaus, M., Duffy, J.E., Barry, J.P., Chan, F., English, C.A., Galindo, H.M., Grebmeier, J.M., Hollowed, A.B., Knowlton, N., Polovina, J., 2011. Climate change impacts on marine ecosystems.

Dong, B., Sutton, R.T., Scaife, A.A., 2006. Multidecadal modulation of El Niño–Southern Oscillation (ENSO) variance by Atlantic Ocean sea surface temperatures. *Geophysical Research Letters*, *33*(8).

Donlon, C. J., Martin, M., Stark, J., Roberts-Jones, J., Fiedler, E., Wimmer, W., 2012. The operational sea surface temperature and sea ice analysis (OSTIA) system. *Remote Sensing of Environment*, *116*, pp.140-158.

Dorman, C.E., Winant, C.D., 2000. The structure and variability of the marine atmosphere around the Santa Barbara Channel. *Monthly Weather Review*, *128*(2), pp.261-282.

Dufois, F., Penven, P., Whittle, C.P., Veitch, J., 2012. On the warm nearshore bias in Pathfinder monthly SST products over Eastern Boundary Upwelling Systems. *Ocean Modelling*, *47*, pp.113-118.

Echevin, V., Albert, A., Lévy, M., Graco, M., Aumont, O., Piétri, A., Garric, G., 2014. Intraseasonal variability of nearshore productivity in the Northern Humboldt Current System: The role of coastal trapped waves. *Continental Shelf Research*, *73*, pp.14-30.

Escribano, R., Daneri, G., Farías, L., Gallardo, V.A., González, H.E., Gutiérrez, D., Lange, C.B., Morales, C.E., Pizarro, O., Ulloa, O., Braun, M., 2004. Biological and chemical consequences of the 1997–1998 El Niño in the Chilean coastal upwelling system: a synthesis. *Deep Sea Research Part II: Topical Studies in Oceanography*, *51*(20-21), pp.2389-2411.

Espinoza-Morriberón, D., Echevin, V., Colas, F., Tam, J., Ledesma, J., Vásquez, L., Graco, M., 2017. Impacts of E l N iño events on the P eruvian upwelling system productivity. *Journal of Geophysical Research: Oceans*, *122*(7), pp.5423-5444.

Fennel, W., 1999. Theory of the Benguela upwelling system. *Journal of Physical Oceanography*, *29*(2), pp.177-190.

Fielding, P. J., Davis, C. L., 1989. Carbon and nitrogen resources available to kelp bed filter feeders in an upwelling environment. *Marine Ecology Progress Series*, pp.181-189.

Florenchie, P., Reason, C.J.C., Lutjeharms, J.R.E., Rouault, M., Roy, C., Masson, S., 2004. Evolution of interannual warm and cold events in the southeast Atlantic Ocean. *Journal of Climate*, *17*(12), pp.2318-2334.

Fogt, R.L. and Bromwich, D.H., 2006. Decadal variability of the ENSO teleconnection to the high-latitude South Pacific governed by coupling with the southern annular mode. *Journal of Climate*, *19*(6), pp.979-997.

Fréon, P., Arístegui, J., Bertrand, A., Crawford, R.J., Field, J.C., Gibbons, M.J., Tam, J., Hutchings, L., Masski, H., Mullon, C., Ramdani, M., 2009. Functional group biodiversity in Eastern Boundary Upwelling Ecosystems questions the wasp-waist trophic structure. *Progress in Oceanography*, *83*(1-4), pp.97-106.

Finkelstein, P.L., 1981. "Measuring the dynamic performance of wind vanes." *Journal of Applied Meteorology* 20, no. 5: 588-594.

García-Reyes, M., Largier, J., 2010. Observations of increased wind-driven coastal upwelling off central California. *Journal of Geophysical Research: Oceans*, *115*(C4).

García-Reyes, M., Sydeman, W.J., Schoeman, D.S., Rykaczewski, R.R., Black, B.A., Smit, A.J., Bograd, S.J., 2015. Under pressure: climate change, upwelling, and eastern boundary upwelling ecosystems. *Frontiers in Marine Science*, *2*, p.109.

Garreaud, R.D., Falvey, M., 2009. The coastal winds off western subtropical South America in future climate scenarios. *International Journal of Climatology: A Journal of the Royal Meteorological Society*, *29*(4), pp.543-554.

Gillett, N.P., Fyfe, J.C., Parker, D.E., 2013. Attribution of observed sea level pressure trends to greenhouse gas, aerosol, and ozone changes. *Geophysical Research Letters*, *40*(10), pp.2302-2306.

Graco, M.I., Purca, S., Dewitte, B., Castro, C.G., Morón, O., Ledesma, J., Flores, G., Gutiérrez, D., 2017. The OMZ and nutrient features as a signature of interannual and low-frequency variability in the Peruvian upwelling system.

Grise, K.M., Davis, S.M., Simpson, I.R., Waugh, D.W., Fu, Q., Allen, R.J., Rosenlof, K.H., Ummenhofer, C.C., Karnauskas, K.B., Maycock, A.C. and Quan, X.W., 2019. Recent tropical expansion: Natural variability or forced response?. *Journal of Climate*, *32*(5), pp.1551-1571.

Grise, K.M. and Davis, S.M., 2020. Hadley cell expansion in CMIP6 models. *Atmospheric Chemistry & Physics*, *20*(9).

Guastella, L.A., 1992. Sea surface heat exchange at St Helena Bay and implications for the southern Benguela upwelling system. South African Journal of Marine Science, 12(1), pp.61-70.

Gruber, N., Lachkar, Z., Frenzel, H., Marchesiello, P., Münnich, M., McWilliams, J.C., Nagai, T., Plattner, G.K., 2011. Eddy-induced reduction of biological production in eastern boundary upwelling systems. *Nature geoscience*, *4*(11), pp.787-792.

Guastella, L.A., 1992. Sea surface heat exchange at St Helena Bay and implications for the southern Benguela upwelling system. *South African Journal of Marine Science*, *12*(1), pp.61-70.

Gutknecht, E., Dadou, I., Marchesiello, P., Cambon, G., Le Vu, B., Sudre, J., Garçon, V., Machu, E., Rixen, T., Kock, A., Flohr, A., 2013. Nitrogen transfers off Walvis Bay: a 3-D coupled physical/biogeochemical modeling approach in the Namibian upwelling system. *Biogeosciences*, *10*(6), pp.4117-4135.

Haack, T., Chelton, D., Pullen, J., Doyle, J.D., Schlax, M., 2008. Summertime influence of SST on surface wind stress off the US West Coast from the US Navy COAMPS model. *Journal of physical oceanography*, *38*(11), pp.2414-2437.

Hagen, E., 2009. Atlantic Exploration and Climate. *Selected Contributions on Results of Climate Research in East Germany*, pp.80-95.

Hall, D.K., Comiso, J.C., DiGirolamo, N.E., Shuman, C.A., Key, J.R. and Koenig, L.S., 2012. A satellite-derived climate-quality data record of the clear-sky surface temperature of the Greenland ice sheet. *Journal of Climate*, *25*(14), pp.4785-4798.

Halpern, D., 2002. Offshore Ekman transport and Ekman pumping off Peru during the 1997–1998 El Nino. *Geophysical Research Letters*, *29*(5), pp.19-1.

Harlass, J., Latif, M., Park, W., 2015. Improving climate model simulation of tropical Atlantic sea surface temperature: The importance of enhanced vertical atmosphere model resolution. *Geophysical Research Letters*, *42*(7), pp.2401-2408.

Harley, C.D., Randall Hughes, A., Hultgren, K.M., Miner, B.G., Sorte, C.J., Thornber, C.S., Rodriguez, L.F., Tomanek, L., Williams, S.L., 2006. The impacts of climate change in coastal marine systems. *Ecology letters*, *9*(2), pp.228-241.

Hausfather, Z., Cowtan, K., Menne, M.J., Williams Jr, C.N., 2016. Evaluating the impact of US historical climatology network homogenization using the US climate reference network. *Geophysical Research Letters*, *43*(4), pp.1695-1701.

Hoegh-Guldberg, O., Bruno, J.F., 2010. The impact of climate change on the world's marine ecosystems. *Science*, *328*(5985), pp.1523-1528.

Holbrook, N.J., Goodwin, I.D., McGregor, S., Molina, E. and Power, S.B., 2011. ENSO to multi-decadal time scale changes in East Australian Current transports and Fort Denison sea level: Oceanic Rossby waves as the connecting mechanism. *Deep Sea Research Part II: Topical Studies in Oceanography*, *58*(5), pp.547-558.

Hutchings, L., Van der Lingen, C. D., Shannon, L. J., Crawford, R. J. M., Verheye, H. M. S., Bartholomae, C. H., Van der Plas, A. K., Louw, D., Kreiner, A., Ostrowski, M., Fidel, Q., 2009. The Benguela Current: An ecosystem of four components. *Progress in Oceanography*, *83*(1-4), pp.15-32.

Huyer, A., 1983. Coastal upwelling in the California Current system. *Progress in oceanography*, *12*(3), pp.259-284.

Hsieh, W.W., Boer, G.J., 1992. Global climate change and ocean upwelling. *Fisheries Oceanography*, *1*(4), pp.333-338.

Jacox, M.G., Fiechter, J., Moore, A.M., Edwards, C.A., 2015. ENSO and the C alifornia C urrent coastal upwelling response. *Journal of Geophysical Research: Oceans*, *120*(3), pp.1691-1702.

Jakoboski, J., Todd, R.E., Owens, W.B., Karnauskas, K.B., Rudnick, D.L., 2020. Bifurcation and upwelling of the equatorial undercurrent west of the Galapagos archipelago. *Journal of Physical Oceanography*, *50*(4), pp.887-905.

Jury, M.R., 1980. Characteristics of summer wind field and air sea interaction over the Cape Peninsula upwelling regions. M.Sc. Thesis. University of Cape Town, South Africa.

Kennedy, J.J., Rayner, N.A., Smith, R.O., Parker, D.E., Saunby, M., 2011. Reassessing biases and other uncertainties in sea surface temperature observations measured in situ since 1850: 1. Measurement and sampling uncertainties. *Journal of Geophysical Research: Atmospheres*, *116*(D14).

Kessler, W.S., 2002. Is ENSO a cycle or a series of events?. *Geophysical Research Letters*, *29*(23), pp.40-1.

Kilpatrick, K.A., Podesta, G.P., Evans, R., 2001. Overview of the NOAA/NASA advanced very high resolution radiometer Pathfinder algorithm for sea surface temperature and associated matchup database. *Journal of Geophysical Research: Oceans*, *106*(C5), pp.9179-9197.

Klein, S.A., Soden, B.J., Lau, N.C., 1999. Remote sea surface temperature variations during ENSO: Evidence for a tropical atmospheric bridge. *Journal of climate*, *12*(4), pp.917-932.

Lau, N.C., 1997. Interactions between global SST anomalies and the midlatitude atmospheric circulation. *Bulletin of the American Meteorological Society*, *78*(1), pp.21-34.

Liu, Y. and Minnett, P.J., 2016. Sampling errors in satellite-derived infrared sea-surface temperatures. Part I: Global and regional MODIS fields. *Remote sensing of environment*, *177*, pp.48-64.

Lima, F.P., Wethey, D.S., 2012. Three decades of high-resolution coastal sea surface temperatures reveal more than warming. *Nature communications*, *3*(1), pp.1-13.

Lu, F., Hu, H., Sun, W., Zhu, J., Liu, G., Zhou, W., Zhang, Q., Shi, P., Liu, X., Wu, X., Zhang, L., 2018. Effects of national ecological restoration projects on carbon sequestration in China from 2001 to 2010. *Proceedings of the National Academy of Sciences*, *115*(16), pp.4039-4044.

McGregor, H.V., Dima, M., Fischer, H.W. and Mulitza, S., 2007. Rapid 20th-century increase in coastal upwelling off northwest Africa. *science*, *315*(5812), pp.637-639.

Mead, A., Griffiths, C.L., Branch, G.M., McQuaid, C.D., Blamey, L.K., Bolton, J.J., Anderson, R.J., Dufois, F., Rouault, M., Froneman, P.W., Whitfield, A.K., 2013. Human-mediated drivers of change—impacts on coastal ecosystems and marine biota of South Africa. *African Journal of Marine Science*, *35*(3), pp.403-425.

Menne, M.J., Williams Jr, C.N., Vose, R.S., 2009. The US Historical Climatology Network monthly temperature data, version 2. *Bulletin of the American Meteorological Society*, *90*(7), pp.993-1008.

Mesias, J.M., Bisagni, J.J. and Brunner, A.M., 2007. A high-resolution satellite-derived sea surface temperature climatology for the western North Atlantic Ocean. *Continental Shelf Research*, *27*(2), pp.191-207.

Messié, M., Ledesma, J., Kolber, D.D., Michisaki, R.P., Foley, D.G., Chavez, F.P., 2009. Potential new production estimates in four eastern boundary upwelling ecosystems. *Progress in Oceanography*, *83*(1-4), pp.151-158.

Minnett, P.J., 1991. Consequences of sea surface temperature variability on the validation and applications of satellite measurements. *Journal of Geophysical Research: Oceans*, *96*(C10), pp.18475-18489.

Minnett, P.J., Brown, O.B., Evans, R.H., Key, E.L., Kearns, E.J., Kilpatrick, K., Kumar, A., Maillet, K.A. and Szczodrak, G., 2004, September. Sea-surface temperature measurements from the Moderate-Resolution Imaging Spectroradiometer (MODIS) on Aqua and Terra. In *IGARSS 2004. 2004 IEEE International Geoscience and Remote Sensing Symposium* (Vol. 7, pp. 4576-4579). Ieee.

Morales, C.E., Hormazábal, S.E., Blanco, J., 1999. Interannual variability in the mesoscale distribution of the depth of the upper boundary of the oxygen minimum layer off northern Chile (18–24S): Implications for the pelagic system and biogeochemical cycling. Journal of Marine Research, 57(6), pp.909-932.

Montecino, V., Rutllant, J., Salinas, S., 2005. Coastal ocean circulation off western South America. *The Global Coastal Ocean-Regional Studies and Syntheses*, *11*, p.273.

Montecino, V., Lange, C.B., 2009. The Humboldt Current System: Ecosystem components and processes, fisheries, and sediment studies. *Progress in Oceanography*, *83*(1-4), pp.65-79.

Morales, C.E., Hormazábal, S.E., Blanco, J., 1999. Interannual variability in the mesoscale distribution of the depth of the upper boundary of the oxygen minimum layer off northern Chile (18–24S): Implications for the pelagic system and biogeochemical cycling. *Journal of Marine Research*, *57*(6), pp.909-932.

Mote, P.W., Mantua, N.J., 2002. Coastal upwelling in a warmer future. *Geophysical research letters*, *29*(23), pp.53-1.

Mote, P.W., Salathé, E.P., 2010. Future climate in the Pacific Northwest. *Climatic change*, *102*(1-2), pp.29-50.

Murawski, S.A., 1993. Climate change and marine fish distributions: forecasting from historical analogy. *Transactions of the American Fisheries Society*, *122*(5), pp.647-658.

Narayan, N., 2010. Interactive comment on "Trends in coastal upwelling intensity during the late 20th century" by N. Narayan et al.

Nelson, G., Hutchings, L., 1983. The Benguela upwelling area. *Progress in Oceanography*, *12*(3), pp.333-356.

Pardo, P.C., Padín, X.A., Gilcoto, M., Farina-Busto, L., Pérez, F.F., 2011. Evolution of upwelling systems coupled to the long-term variability in sea surface temperature and Ekman transport. *Climate Research*, *48*(2-3), pp.231-246.

Parker, D.E., Folland, C.K., Jackson, M., 1995. Marine surface temperature: observed variations and data requirements. *Climatic Change*, *31*(2-4), pp.559-600.

Pauly, D., Christensen, V., 1995. Primary production required to sustain global fisheries. Nature, 374(6519), pp.255-257.

Pegliasco, C., Chaigneau, A., Morrow, R., 2015. Main eddy vertical structures observed in the four major Eastern Boundary Upwelling Systems. *Journal of Geophysical Research: Oceans*, *120*(9), pp.6008-6033.

Pelegrí, J.L., Peña-Izquierdo, J., 2015. Inorganic nutrients and dissolved oxygen in the Canary Current Large Marine Ecosystem.

Peterson, W.T., Schwing, F.B., 2003. A new climate regime in northeast Pacific ecosystems. *Geophysical research letters*, *30*(17).

Perlin, N., Samelson, R.M., Chelton, D.B., 2004. Scatterometer and model wind and wind stress in the Oregon–northern California coastal zone. *Monthly Weather Review*, *132*(8), pp.2110-2129.

Perlin, N., Skyllingstad, E.D., Samelson, R.M., 2010. Coastal Atmospheric Circulation around a Cape and its Response to Wind-Driven Upwelling Studied Using a Coupled Ocean-Atmosphere Model.

Perlin, N., Skyllingstad, E.D., Samelson, R.M., 2011. Coastal atmospheric circulation around an idealized cape during wind-driven upwelling studied from a coupled ocean–atmosphere model. *Monthly Weather Review*, *139*(3), pp.809-829.

Rahmstorf, S., 2002. Ocean circulation and climate during the past 120,000 years. *Nature*, *419*(6903), pp.207-214.

Rasmusson, E.M., Carpenter, T.H., 1982. Variations in tropical sea surface temperature and surface wind fields associated with the Southern Oscillation/El Niño. *Monthly Weather Review*, *110*(5), pp.354-384.

Rayner, N.A., Brohan, P., Parker, D.E., Folland, C.K., Kennedy, J.J., Vanicek, M., Ansell, T.J. and Tett, S.F.B., 2006. Improved analyses of changes and uncertainties in sea surface temperature measured in situ since the mid-nineteenth century: The HadSST2 dataset. *Journal of Climate*, *19*(3), pp.446-469.

Reynolds, R.W., Smith, T.M., 1994. Improved global sea surface temperature analyses using optimum interpolation. *Journal of climate*, *7*(6), pp.929-948.

Reynolds, R.W., Smith, T.M., 1995. A high-resolution global sea surface temperature climatology. *Journal of Climate*, *8*(6), pp.1571-1583.

Reynolds, R.W., Rayner, N.A., Smith, T.M., Stokes, D.C., Wang, W., 2002. An improved in situ and satellite SST analysis for climate. *Journal of climate*, *15*(13), pp.1609-1625.

Reynolds, R.W., Chelton, D.B., 2010. Comparisons of daily sea surface temperature analyses for 2007–08. *Journal of climate*, *23*(13), pp.3545-3562.

Reynolds, R.W., Chelton, D.B., Roberts-Jones, J., Martin, M.J., Menemenlis, D., Merchant, C.J., 2013. Objective determination of feature resolution in two sea surface temperature analyses. *Journal of climate*, *26*(8), pp.2514-2533.

Ricciardulli, L., Wentz, F.J., 2004. Uncertainties in sea surface temperature retrievals from space: Comparison of microwave and infrared observations from TRMM. *Journal of Geophysical Research: Oceans*, *109*(C12).

Rimbu, N., Lohmann, G., Kim, J.H., Arz, H.W., Schneider, R., 2003. Arctic/North Atlantic Oscillation signature in Holocene sea surface temperature trends as obtained from alkenone data. *Geophysical research letters*, *30*(6).

Risien, C.M., Reason, C.J.C., Shillington, F.A., Chelton, D.B., 2004. Variability in satellite winds over the Benguela upwelling system during 1999–2000. *Journal of Geophysical Research: Oceans*, *109*(C3).
Robinson, I. S., Wells, N. C. and Charnock, H. (1984). The sea surface thermal boundary layer and its relevance to the measurement of sea surface temperature by airborne and spaceborne radiometers. *International Journal of Remote Sensing*, *5*(1), pp.19-45.

Roemmich, D., McGowan, J., 1995. Climatic warming and the decline of zooplankton in the California Current. *Science*, *267*(5202), pp.1324-1326.

Rossi, V., 2010. *Influence of mesoscale physical processes on planktonic ecosystems in the regional ocean: application to the Eastern Boundary Upwelling Systems* (Doctoral dissertation).

Rouault, M., Florenchie, P., Fauchereau, N., Reason, C.J., 2003. South East tropical Atlantic warm events and southern African rainfall. *Geophysical Research Letters*, *30*(5).

Rouault, M., Pohl, B., Penven, P., 2010. Coastal oceanic climate change and variability from 1982 to 2009 around South Africa. *African Journal of Marine Science*, *32*(2), pp.237-246.

Rykaczewski, R.R., Dunne, J.P., Sydeman, W.J., García-Reyes, M., Black, B.A., Bograd, S.J., 2015. Poleward displacement of coastal upwelling-favorable winds in the ocean's eastern boundary currents through the 21st century. *Geophysical Research Letters*, *42*(15), pp.6424-6431.

Saji, N.H., Goswami, B.N., Vinayachandran, P.N. and Yamagata, T., 1999. A dipole mode in the tropical Indian Ocean. *Nature*, *401*(6751), pp.360-363.

Samanta, D., Karnauskas, K.B., Goodkin, N.F., 2019. Tropical Pacific SST and ITCZ biases in climate models: Double trouble for future rainfall projections?. *Geophysical Research Letters*, *46*(4), pp.2242-2252.

Santos, F., Gomez-Gesteira, M., Decastro, M., Alvarez, I., 2012. Differences in coastal and oceanic SST trends due to the strengthening of coastal upwelling along the Benguela current system. *Continental Shelf Research*, *34*, pp.79-86.

Seabra, R., Varela, R., Santos, A.M., Gómez-Gesteira, M., Meneghesso, C., Wethey, D.S., Lima, F.P., 2019. Reduced nearshore warming associated with eastern boundary upwelling systems. *Frontiers in Marine Science*, *6*, p.104.

Schlegel, R.W., Smit, A.J., 2016. Climate change in coastal waters: time series properties affecting trend estimation. *Journal of Climate*, *29*(24), pp.9113-9124.

Schlegel, R.W., Oliver, E.C., Perkins-Kirkpatrick, S., Kruger, A., Smit, A.J., 2017. Predominant atmospheric and oceanic patterns during coastal marine heatwaves. *Frontiers in Marine Science*, *4*, p.323.

Schlegel, R.W., Smit, A.J., 2018. heatwaveR: a central algorithm for the detection of heatwaves and cold-spells. *Journal of Open Source Software*, *3*(27), p.821.

Schultz, O.J., 2010. *Belonging to the West Coast: an ethnography of St Helena Bay in the context of marine resource scarcity* (Doctoral dissertation, University of Cape Town).

Scoccimarro, E., Gualdi, S., Bellucci, A., Sanna, A., Giuseppe Fogli, P., Manzini, E., Vichi, M., Oddo, P., Navarra, A., 2011. Effects of tropical cyclones on ocean heat transport in a high-resolution coupled general circulation model. *Journal of Climate*, *24*(16), pp.4368-4384.

Servain, J., Picaut, J., Busalacchi, A.J., 1985. Interannual and seasonal variability of the tropical Atlantic Ocean depicted by sixteen years of sea-surface temperature and wind stress. In *Elsevier oceanography series* (Vol. 40, pp. 211-237). Elsevier.

Shaffer, G., Pizarro, O., Djurfeldt, L., Salinas, S., Rutllant, J., 1997. Circulation and low-frequency variability near the Chilean coast: Remotely forced fluctuations during the 1991–92 El Nino. *Journal of Physical Oceanography*, *27*(2), pp.217-235.

Shannon, L.V., 1985. The Benguela ecosystem. I: Evolution of the Benguela physical features and processes. Oceanography and Marine Biology, 23, pp.105-182.

Shannon, L.V., Boyd, A.J., Brundrit, G.B., Taunton-Clark, J., 1986. On the existence of an El Niño-type phenomenon in the Benguela system. *Journal of marine Research*, *44*(3), pp.495-520.

Smith, T.M., Reynolds, R.W., 1998. A high-resolution global sea surface temperature climatology for the 1961–90 base period. *Journal of Climate*, *11*(12), pp.3320-3323.

Smit, A.J., Roberts, M., Anderson, R.J., Dufois, F., Dudley, S.F., Bornman, T.G., Olbers, J., Bolton, J.J., 2013. A coastal seawater temperature dataset for biogeographical studies: large biases between in situ and remotely-sensed data sets around the coast of South Africa. *PLoS One*, *8*(12).

Snyder, M.A., Sloan, L.C., Diffenbaugh, N.S., Bell, J.L., 2003. Future climate change and upwelling in the California Current. *Geophysical Research Letters*, *30*(15).

Sohn, B.J., Yeh, S.W., Schmetz, J. and Song, H.J., 2013. Observational evidences of Walker circulation change over the last 30 years contrasting with GCM results. *Climate Dynamics*, *40*(7-8), pp.1721-1732.

Stenseth, N.C., Mysterud, A., Ottersen, G., Hurrell, J.W., Chan, K.S., Lima, M., 2002. Ecological effects of climate fluctuations. *Science*, *297*(5585), pp.1292-1296.

Stander, G.H., De Decker, A.H.B., 1969. *Some physical and biological aspects of an oceanographic anomaly off South West Africa in 1963*. Department of Commerce, Division of Fisheries.

Stocker, T.F., Qin, D., Plattner, G.K., Tignor, M., Allen, S.K., Boschung, J., Nauels, A., Xia, Y., Bex, V., Midgley, P.M., 2013. Climate change 2013: The physical science basis. *Contribution of working group I to the fifth assessment report of the intergovernmental panel on climate change*, *1535*.

Sutton, R.T., Jewson, S.P., Rowell, D.P., 2000. The elements of climate variability in the tropical Atlantic region. *Journal of Climate*, *13*(18), pp.3261-3284.

Sydeman, W.J., Santora, J.A., Thompson, S.A., Marinovic, B., Lorenzo, E.D., 2013. Increasing variance in North Pacific climate relates to unprecedented ecosystem variability off California. *Global Change Biology*, *19*(6), pp.1662-1675.

Sydeman, W.J., García-Reyes, M., Schoeman, D.S., Rykaczewski, R.R., Thompson, S.A., Black, B.A., Bograd, S.J., 2014. Climate change and wind intensification in coastal upwelling ecosystems. *Science*, *345*(6192), pp.77-80.

Sverdrup, H.U., Allen, W.E., 1939. Distribution of diatoms in relation to the character of water masses and currents off southern California in 1938. *J. mar. Res*, *2*(2), pp.131-144.

Tang, D., Dana, R.K., Zhaoding, W., Jiansheng, L., Hiroshi, K., 2003. "AVHRR satellite remote sensing and shipboard measurements of the thermal plume from the Daya Bay, nuclear power station, China." *Remote Sensing of Environment* 84, no. 4: 506-515.

Tim, N., Zorita, E., Hünicke, B., 2015. Decadal variability and trends of the Benguela upwelling system as simulated in a high-resolution ocean simulation. *Ocean Sci*, *11*(3), pp.483-502.

Timmermann, A., Oberhuber, J., Bacher, A., Esch, M., Latif, M., Roeckner, E., 1999. Increased El Niño frequency in a climate model forced by future greenhouse warming. *Nature*, *398*(6729), pp.694-697.

Tittensor, D.P., Mora, C., Jetz, W., Lotze, H.K., Ricard, D., Berghe, E.V., Worm, B., 2010. Global patterns and predictors of marine biodiversity across taxa. *Nature*, *466*(7310), pp.1098-1101.

Tyson, P.D., Preston-Whyte, R.A., 2000. *Weather and climate of southern Africa*. Oxford University Press.

Ulloa, O., Escribano, R., Hormazabal, S., Quinones, R.A., González, R.R., Ramos, M., 2001. Evolution and biological effects of the 1997–98 El Nino in the upwelling ecosystem off northern Chile. *Geophysical Research Letters*, *28*(8), pp.1591-1594.

Vallis, G.K., 1986. El Niño: A chaotic dynamical system?. *Science*, *232*(4747), pp.243-245.

Van Heerden, J., Hurry, L., 1998. Southern Africa's weather patterns: An introductory guide. Collegium.

Vargas, G., Pantoja, S., Rutllant, J.A., Lange, C.B., Ortlieb, L., 2007. Enhancement of coastal upwelling and interdecadal ENSO-like variability in the Peru-Chile Current since late 19th century. *Geophysical Research Letters*, *34*(13).

Walker, A., 2020. *Observed Trends of Coastal Upwelling in Eastern Boundary Upwelling Systems* (Doctoral dissertation, University of Colorado at Boulder).

Wang, W., McPhaden, M.J., 2000. The surface-layer heat balance in the equatorial Pacific Ocean. Part II: Interannual variability. *Journal of Physical Oceanography*, *30*(11), pp.2989-3008.

Wang, C., 2004. ENSO, Atlantic climate variability, and the Walker and Hadley circulations. In *The Hadley circulation: Present, past and future* (pp. 173-202). Springer, Dordrecht.

Wang, X.L., Cai, X.D., Su, Z.E., Chen, M.C., Wu, D., Li, L., Liu, N.L., Lu, C.Y., Pan, J.W., 2015. Quantum teleportation of multiple degrees of freedom of a single photon. *Nature*, *518*(7540), pp.516-519.

Whitfield, A.K., James, N.C., Lamberth, S.J., Adams, J.B., Perissinotto, R., Rajkaran, A., Bornman, T.G., 2016. The role of pioneers as indicators of biogeographic range expansion caused by global change in southern African coastal waters. *Estuarine, Coastal and Shelf Science*, *172*, pp.138-153.

Wick, G.A., Emery, W.J., Schluessel, P., 1992. A comprehensive comparison between satellite-measured skin and multichannel sea surface temperature. *Journal of Geophysical Research: Oceans*, *97*(C4), pp.5569-5595.

Wycech, J.B., Gill, E., Rajagopalan, B., Marchitto Jr, T.M., Molnar, P.H., 2020. Multiproxy Reduced-Dimension Reconstruction of Pliocene Equatorial Pacific Sea Surface Temperatures. *Paleoceanography and Paleoclimatology*, *35*(1), p.e2019PA003685.

Yeh, S.W., Cai, W., Min, S.K., McPhaden, M.J., Dommenget, D., Dewitte, B., Collins, M., Ashok, K., An, S.I., Yim, B.Y. and Kug, J.S., 2018. ENSO atmospheric teleconnections and their response to greenhouse gas forcing. *Reviews of Geophysics*, *56*(1), pp.185-206.

Zebiak, S.E., 1993. Air–sea interaction in the equatorial Atlantic region. *Journal of Climate*, *6*(8), pp.1567-1586.

Zhang, L., Han, W., Karnauskas, K.B., Meehl, G.A., Hu, A., Rosenbloom, N., Shinoda, T., 2019. Indian Ocean warming trend reduces Pacific warming response to anthropogenic greenhouse gases: An interbasin thermostat mechanism. *Geophysical Research Letters*, *46*(19), pp.10882-10890.